Widespread poly-metamorphosed Archean granitoid gneisses and supracrustal enclaves of the southern Inukjuak Domain, Québec (Canada)

Jennika Greer, Guillaume Caro, Nicole L Cates, Peter Tropper, Wouter Bleeker, Nigel M Kelly, Stephen J Mojzsis

Widespread poly-metamorphosed Archean granitoid gneisses and supracrustal enclaves of the southern Inukjuak Domain, Québec (Canada).

Jennika Greer[1,2,3], Guillaume Caro[4], Nicole L. Cates[1,5], Peter Tropper[6], Wouter Bleeker[7], Nigel M. Kelly[1†] and Stephen J. Mojzsis[1,8*]

[1.] *Department of Geological Sciences, University of Colorado, 2200 Colorado Avenue, Boulder, CO 80309-0399, USA* mojzsis@colorado.edu

[2.] *Department of the Geophysical Sciences, Chicago Center for Cosmochemistry, University of Chicago, Chicago, IL, USA* jennika@uchicago.edu

[3.] *Robert A. Pritzker Center for Meteoritics and Polar Studies, Field Museum of Natural History, Chicago, IL, USA*

[4.] *Centre de Recherches Pétrographiques et Géochimiques (CRPG), UMR 7358, Université de Lorraine, CNRS, 54500 Vandoeuvre-lès-Nancy, France* caro@crpg.cnrs-nancy.fr

[5.] *Department of Geological Sciences, University of Manitoba, 240 Wallace Building, 125 Dysart Road, Winnipeg, MB R3T 2N2, Canada* nlcates@gmail.com

[6.] *Institute of Mineralogy and Petrography, University of Innsbruck, Innrain 52, A-6020 Innsbruck, Austria* peter.tropper@uibk.ac.at

[7.] *Geological Survey of Canada, 601 Booth Street, Ottawa, Ontario K1A 0E8, Canada* wouter.bleeker@canada.ca

[8.] *Institute for Geological and Geochemical Research, RCAES, Hungarian Academy of Sciences, 1112 Budapest, Budaörsi u. 45, Hungary*

[†]*Present address: Bruker Nano Analytics, Am Studio 2D, 12489 Berlin, Germany* nigel.kelly@bruker.com

[*] *Corresponding author:* mojzsis@colorado.edu

Abstract: 380 words
Main Text: 8535 words
Figures: 14
Tables: 0
References: 58
Supplementary Information: 7 Figures, 4 Tables

Keywords
Archean; Inukjuak; supracrustal belt; granitoid gneisses; geochronology; metamorphic petrology

Highlights

1. The Inukjuak Domain comprises ~12,000 km^2 of Eo- to Neoarchean gneisses, (ultra)mafic schists and supracrustal enclaves within the Minto Block of northern Québec.

2. At least four generations of variably deformed Archean granite-granitoid gneisses are documented.

3. The oldest enclosing granodioritic and trondjemitic gneisses are ca. 3800 Ma; in some cases, these structurally transect supracrustal rocks and establish minimum ages.

4. Innuksuac Complex supracrustal enclaves range in size from <1 m^2 to ~10 km^2 and show a variety of protolith compositions.

5. The terrane is metamorphosed to amphibolite facies with local retrogressions, reflecting a protracted history that precludes preservation of primary fine-scale (microfossil) structures.

Abstract. The ~12,000 km^2 Inukjuak Domain in northern Québec is part of the Archean Minto Block in the northwestern Superior Province of Canada. Eoarchean (ca. >3800-3780 Ma) rocks of the Nuvvuagittuq supracrustal belt (NSB) are the best known occurrence of otherwise abundant <1 m to km-scale supracrustal enclaves dispersed throughout the Innuksuac Complex. The supracrustals are dominantly amphibolites, with subordinate intermediate-, mafic- and ultramafic schists, quartzo-feldspathic (trondhjemitic and granodioritic) sills, dikes and sheets, banded iron-formations and quartz-pyroxene±magnetite rocks, and (detrital) fuchsitic quartzites. Supracrustal assemblages are in turn hosted by variably deformed granite-granitoid gneisses metamorphosed to amphibolite facies. Locally, retrogression is expressed as pervasive chloritization and development of jaspilite box veinings. This metamorphic history precludes preservation of original fragile microfossil shapes. Despite its importance as one of the few terranes to host Eoarchean supracrustal assemblages, limited geochronology was previously available for rocks beyond the ~8 km^2 NSB. Here, we report new major-, minor-, and trace-element geochemistry and metamorphic petrology coupled with U-Pb zircon geochronology, from rocks within and surrounding the NSB. These include the little-studied but volumetrically significant Voizel suite gneisses. Results show that intra-NSB fold belt rocks of the Central Tonalitic Gneiss (CTG) preserve mainly ca. 3650 Ma zircons. Beyond the NSB, the Voizel gneisses – previously considered contemporaneous with the CTG – are instead about 100 Myr younger (~3550 Ma). Tonalitic (ortho)gneisses at the margin of the NSB were previously assigned a ca. 3650 Ma age, and the surrounding Boizard suite gneisses may be about 2700 Ma. We find the Boizard rocks contain inherited zircon cores up to ca. 3700 Ma, with younger overgrowths dated at ca. 2700 Ma. A tonalitic gneiss that transects another highly deformed supracrustal enclave north of the NSB – dubbed the Ukaliq Supracrustal Belt – yields maximum

concordant zircon ages of 3653 ± 16 Ma (2σ). Detrital zircons from Ukaliq and Nuvvuagittuq quartzites and quartz-biotite schists define a maximum age of ca. 3780 Ma. No indication of U-Pb zircon ages older than about 3800 Ma exist in this terrane. Our reconnaissance sampling of gneisses to the west of the NSB fold belt yielded more zircon-bearing rocks with ages of ca. 3760 Ma. Discovery of more pre-3700 Ma rocks beyond the NSB outcrops calls attention to the existence of widespread scattered occurrences of Eoarchean and Paleoarchean rocks throughout the region. (**380 words**)

1. Introduction

The world's oldest rocks of demonstrably volcano-sedimentary origin comprise the Archean "supracrustal belts"; these typically occur as irregularly deformed and metamorphosed enclaves and rafts with broad spectrum of sizes captured in ancient granite-granitoid gneiss terranes that are in turn separated unconformably from the surrounding felsic cratonic basement rocks (e.g., de Wit and Ashwal, 1995). Although such bodies tend to be bounded by shear zones, examples also exist of Archean crustal enclaves that preserve weathering horizons and basal conglomerates, and quartzites, which unconformably rest on old tonalite-trondhjemite-granodiorite (TTG) gneisses (e.g. Bleeker, 2002). Ranging in size from centimeter-scale to tens of kilometers in outcrop area, the various Eoarchean (3850-3600 Ma) supracrustals thus far documented are dominantly amphibolitic. Because of their widely documented poly-phase metamorphic histories, it is a misnomer to refer to these – either at the well-known Isua locality in West Greenland (Nutman et al. 1996), the paragneisses of the Saglek Harbor rocks of Labrador (Schiøtte et al., 1989), or for that matter in the Inukjuak region in northern Québec

described herein – as "greenstone belts" (cf. O'Neil et al. 2007). That is because *without known exception*, all Eoarchean rocks experienced at least one (or more commonly, several) peak mid- to upper-amphibolite (or in some cases granulite facies) metamorphic events with associated recrystallization(s) and several episodes of deformation before undergoing locally highly variable retrogression (e.g. Nutman et al. 2007; Cates and Mojzsis, 2006, 2009; Manning et al. 2006). It is owing to the intense structural juxtaposition of Eoarchean supracrustal rocks with TTG gneisses in the Paleoarchean, followed by terrane assembly, that all such rocks are so strongly modified. As such, none of these rocks are "greenstones" in the strict sense, nor do they hold much potential for preservation of ultrafine-scale primary sedimentary features such as fragile microfossil shapes (Bridgwater et al. 1981; Whitehouse et al. 2019; cf. Dodd et al. 2017). In spite of the fact that all of the oldest (>3.7 Ga) supracrustal rocks are undoubtedly modified due to their long residence times in the crust, they nevertheless constitute the only direct sources of evidence – albeit strongly debated – for the early biological evolution of our planet (e.g., Schidlowski, 1988; Mojzsis et al. 1996; Rosing 1999; Nutman et al. 2016). We come back to significance of this metamorphic history and what it means in the context of origin of life studies in Sections 4.1 & 4.5.

We emphasize that these rocks are so important to our understanding of the nature of the "Early Earth" as a terrane separate from the famous Itsaq Gneiss Complex in southern West Greenland (Nutman et al. 1996) that it makes sense to assess an ancient complex history through enhanced understanding of the gneisses that encompass them. For instance, exploration of surrounding granitoid gneisses can provide minimum ages for the supracrustals where unambiguous field relations exist on cross-cutting dikes, sheets and sills. Extensive surveys of the surrounding granitoids and their ages can also point to thermal peaks in the (poly-

148)metamorphic history endemic to these terranes that can be recapitulated in thermochronological
149 investigations of the supracrustal rocks themselves.
150 One such locality of ancient rocks is the ca. 3750-3780 Ma Nuvvuagittuq supracrustal belt
151 (NSB) in northern Québec (**Figure 1**) (O'Neil et al. 2007, 2019). These were discovered in 2001
152 during a regional geological and geochemical survey sponsored by the Provincial Government of
153 Québec (Simard et al. 2003; David et al. 2003; Stevenson et al. 2005). It should be emphasized
154 that the NSB is merely the best known of what are at least a dozen or so km-scale enclaves in the
155 southern part of the vast (~12,000 km^2) Inukjuak Domain recognizable from aerial photographs
156 available from the offices of Natural Resources Canada and thus mappable at the regional scale
157 (**Figure 2**). Collectively, the assorted supracrustals in the Inukjuak Domain comprise what is
158 termed the Innuksuac Complex (Cates and Mojzsis, 2007, 2009 and references therein).
159 To enhance our understanding of this history, we present new field relations, metamorphic
160 petrographic analysis, geochemical data, and U-Pb zircon geochronology for a selection of rocks
161 within and beyond the NSB that include the little-studied TTG gneisses and associated
162 supracrustal rocks from the nearby Ukaliq supracrustal belt (USB) that was introduced in Caro et
163 al. (2016).
164
165 **2. Geologic background**
166
167 **2.1 Innuksuac Complex supracrustal rocks – Nuvvuagittuq locality**
168 Reviews of the geology of the Nuvvuagittuq supracrustal belt (NSB) are provided elsewhere
169 (O'Neil et al. 2007, 2019 and references therein); a short summary is presented here. The NSB
170 and neighboring supracrustals rocks that compose the Innuksuac Complex are found within the

Inukjuak Domain, which in turn is one of several large deformed belts (e.g., Tikkertuk/Bienville; Minto Lake; Qalluviartuuq/Goudalie; Utsalik) that collectively make up the Minto Block in the northeast Superior province. The Inukjuak Domain is volumetrically dominated by Neoarchean plutonic suites with subordinate rocks of Paleo- to Eoarchean age (**Figure 3**; Simard et al. 2003). The ~8 km^2 outcrop area of the NSB has garnered much interest because of the verified discovery of anomalous deficits in $^{142}Nd/^{144}Nd$ vs. Bulk Silicate Earth (O'Neil et al. 2008; Roth et al. (2013)). Debate continues over the interpretation of these data (e.g. Cates et al. (2013); Roth et al. (2013); Guitreau et al. (2013); Caro et al. (2017), but there is broad agreement that the anomalous $^{142}Nd/^{144}Nd$ values must represent evidence for an early (pre-4300 Ma) separation of the terrestrial silicate reservoirs during the short (half-life = 103 Myr) activity of now-extinct ^{146}Sm (Roth et al. 2013). One school of thought is that the $^{142}Nd/^{144}Nd$ vs. Sm/Nd data, in conjunction with some ancient Sm-Nd model ages, indicate that formation times for certain protoliths to the NSB may be 4300-4400 Ma (O'Neil et al. 2008; 2012; 2019). This interpretation has been challenged, however, by separate studies, and the topic is not discussed further here; instead we refer the reader to Cates et al. (2013), Roth et al. (2013), Guitreau et al. (2013) and Caro et al. (2017). Despite their obvious importance, the NSB rocks specific to the "Porpoise Cove" locality are the only ones mapped at the appropriate detail (i.e., 1:100 scale) to understand a complex and protracted metamorphic history (Cates and Mojzsis, 2009; Cates et al. 2013; cf. O'Neil et al., 2007; Darling et al. 2013).

As has been reviewed elsewhere (Cates and Mojzsis, 2007; O'Neil et al. 2019), the Nuvvuagittuq supracrustals are dominantly composed of (Ca-poor; cummingtonite-rich) basaltic amphibolites. Other rocks include layered ultramafic schists that comprise some rocks with geochemical signatures akin to komatiites (Frank et al. 2016; Touboul et al. 2014), finely-

194 banded quartz magnetite±pyroxene±amphibole rocks (*s.s.* banded iron-formations (BIF);
195 Dauphas et al. 2007; Mloszewska et al. 2012), massive Ca-Fe-Mg silicate "quartzites"
196 (Mloszewska et al. 2013), and quartz-biotite schists of probable detrital origin (Simard et al.
197 2003; Cates and Mojzsis, 2007; O'Neil et al. 2007; David et al. 2009; Cates et al. 2013; Darling
198 et al. 2013; Bell et al. 2018). Cates et al. 2013 proposed that the cummingtonite amphibolite
199 rocks owed their Ca-poor compositions to albitization of pyroclastic debris at time of formation
200 around 3.8 Ga. These authors further argued that the colloquial term "faux amphibolite"
201 endorsed by O'Neil et al. 2009 and others is an unfortunate obfuscation of geologic data.
202 Amphibolitic rocks of such composition are have been noted elsewhere in Eorchean terranes
203 including from southern West Greenland (e.g. sample GR00114 of Manning et al. 2006).
204 Furthermore, it has been detailed that detrital igneous zircons in fuchsitic (Cr-muscovite rich)
205 quartzites and quartz-biotite schists, along with ages for igneous zircons from trondhjemitic
206 gneiss sheets – which in some places structurally transect the supracrustal sequences – show that
207 the NSB is probably not older than ca. 3800 Ma (Cates et al. 2007, 2009, 2013). Even after
208 nearly a thousand published U-Pb zircon ages, very few pre-3900 Ma ages have thus far been
209 identified in the NSB (Bell et al. 2017, 2018). Yet, like many other aspects of the geology of the
210 Nuvvuagittuq rocks, the interpretation that these detrital zircons bracket the maximum age of the
211 NSB at ca. 3800 Ma has also been disputed (Darling et al. 2013; O'Neil et al. 2019).
212
213 **2.2 Innuksuac Complex supracrustal rocks beyond the NSB**
214 A large number of scattered small pods and lenses (<1-10 m), as well as larger (>1 km)
215 supracrustal rafts and enclaves have been provisionally noted within the Inukjuak Domain; the
216 largest of these were tentatively mapped from aerial reconnaissance surveys supplemented by

field studies in the early 2000s (Berclaz et al. 2003). In several aspects, an emulsion-like assortment of locally mappable supracrustal rocks locked within poly-phase granitoid gneisses is not unlike the outcrops of the so-called "Akilia association" found southwards of the Isua area and throughout the Itsaq Gneiss Complex of southern West Greenland (McGregor and Mason, 1977), as well as the lesser-known "Manfred Complex" rocks of the Murchison region of Western Australia (Kinny et al. 1988). Furthermore, much like the type-locality on Akilia (island) for the Akilia association (Nutman et al. 2002; Manning et al. 2006) and other Akilia rocks such as on Innersuartuut in the southern Faeringhavn terrane (Cates and Mojzsis, 2006 and references therein), the Ukaliq rocks are the only other Innuksuac supracrustals in the area beyond Nuvvuagittuq that have mapped in the detail required to understand the field relationships (Caro et al. 2017). Similarly, unlike the large (and arguably coherent) Isua and Nuvvuagittuq belts, those of the Ukaliq, Akilia and Manfred supracrustal enclaves are mostly present in outcrop as a scattered set of volumetrically small ($\leq$1 km^2) and dominantly mafic to ultramafic enclaves, surrounded and broken up by strongly foliated plagiogranitoid gneisses.

Specific to the Inukjuak Domain, the ancient gneisses which host the supracrustals are attributed to the Voizel suite (*Avoi*; Simard et al. 2003). Field relations show that the Voizel suite rocks are further enclosed and disrupted by a pinkish granitoid with only weakly developed tectonic fabric, termed the Bozard suite (*Aboz*). The Bozard rocks were provisionally assigned an age of 2750 ± 5 Ma in published reports from the Ministère des Ressources naturelles, de la Faune et des Parcs (Provincial government of Québec). Evidence exists that the Bozard rocks intrude some supracrustal enclaves in places, for example a pegmatitic dike with the same age was described previously described within the NSB (Simard et al. 2003). The large number of metamorphic zircon growth ages at about 2700 Ma in the NSB imply that the emplacement of

240 the Bozard suite led to regional metamorphism of the Innuksuac complex that variably
241 retrogressed the earlier (Paleoarchean) amphibolite facies metamorphism (Cates and Mojzsis,
242 2007, 2009; Cates et al. 2013; O'Neil et al. 2019).
243
244 **3. Sample collection and analytical methods**
245
246 **3.1 Field relationships**
247 Representative samples of the various rocks associated with the NSB, USB and surrounding
248 terrane (**Figure 4**) were collected by us during the course of regional-scale studies in our 2005,
249 2012, and 2014 field seasons. A subset of these samples was chosen for geochemical analysis
250 based on their apparent lack of weathering and homogeneity at the hand-specimen scale; a
251 further subset was set aside based on perceived likelihood of producing abundant zircons for
252 geochronology.
253
254 **3.2 Petrography**
255 Four representative samples were prepared into thin sections and subsequently investigated
256 using standard optical microscopy and backscatter electron (BSE) images to illustrate the textural
257 relations, as well as by electron microprobe analysis. These samples were specifically chosen for
258 thermobarometry work and provenance studies; see Sections 4.1, 4.5, 4.6).
259
260 **3.3 Whole-rock geochemistry**
261 Samples for whole-rock geochemical analyses were crushed to fine powders at the Rock
262 Preparation Facility in the Department of Geological Sciences at the University of Colorado,

263 Boulder. Dedicated alumina mortars were pre-cleaned with washed quartz sand and conditioned
264 with small amounts of sample before powders were made of the main sample masses. Care was
265 taken to avoid contact with metal hammers, saws, and other metal dividing apparatus that could
266 compromise future isotopic or trace metal analytical work. Splits from homogenized powders
267 were subdivided for major-, minor-, and trace element geochemistry and approximately 40% by
268 mass for each was reserved for archival purposes. Whole-rock geochemical analyses were
269 performed at the CRPG SARM Facility in Nancy (France). Samples for which only geochemical
270 data are presented herein were also analyzed at this Facility.
271
272 **3.4 Ion microprobe U-Pb zircon geochronology**
273 A fraction of those samples targeted for geochronology, based on visual inspection of
274 mineralogy, documented zirconium contents from the geochemical analyses as well as geologic
275 setting, was set aside for zircon extraction. Whole-rock samples were crushed and sieved to <350
276 μm to yield an appropriate size range of zircons. Sieved aliquots were then passed through two
277 stages of standard heavy liquid separations (tetrabromoethane and methylene iodide) with
278 intermediate washings in in reagent-grade acetone by ultra-sonication before final washings in
279 acetone and DI water baths. After drying, strongly ferromagnetic minerals and metal filings
280 fractions were removed with a hand-magnet, followed by separations using a Franz magnetic
281 separator. Individual zircon grains from the least magnetic Franz fraction were then handpicked
282 under a binocular microscope, placed as oriented arrays (common long-axis directions) on
283 double-sided adhesive tape and cast in 2.52 cm-diameter molds with Buehler© epoxide resin
284 along with a halo of grain fragments from zircon standard AS-3 (Paces and Miller, 1993; Black
285 et al. 2003; Cates and Mojzsis, 2009). A variety of zircon sizes and morphologies from each

aliquot was chosen so as to diminish sampling bias. The mounts were cured in a 60°C oven for at least 48 hours prior to the first polishing step. The sample mounts were then polished to brilliance in stages down to 0.25 μm alumina to expose approximate grain centers depending on the grain sizes of the cast fraction. Transmitted and reflected optical micrograph mount maps were produced to facilitate identification and navigation on the mounts. Paired BSE (back-scattered electron) and CL (cathodoluminescence) images (e.g., **Figure 5**; see also **Supplementary Figures S1**) were also acquired for all zircons analyzed for U-Pb to guide primary ion beam position.

Immediately prior to ion microprobe analysis, the zircon mounts were ultrasonically bathed in a 1N HCL solution for several minutes to reduce common Pb contamination, rinsed in ultrapure water, air dried and then sputter-coated with ~100 Å of Au to facilitate conductivity. All U-Pb zircon ion microprobe data were acquired using the UCLA Cameca *ims*1270 high-resolution secondary ion mass spectrometer under standard operating conditions (e.g., Cates et al. 2013). An abridged description of the methods is provided here: a ~8 nA O_2^- primary ion beam was defocused to a ~25 μm diameter spot, and the ion probe was operated at a mass resolving power of ~6000 to exclude molecular interferences. Oxygen flooding to a pressure of 3.2×10^{-5} torr in the analysis chamber was used to increase Pb ion yields (Schuhmacher et al. 1994). Prior to sample (unknown) analysis, a calibration curve was established using the zircon standards 91500 (for set-up) and AS-3 (embedded with the unknowns). Ages for unknown zircons were determined by comparison with a working curve defined by multiple measurements of zircon standard AS3 that yields concordant $^{206}Pb/^{238}U$ and $^{207}Pb/^{235}U$ ages of 1099.1±0.5 Ma. Raw machine data were reduced using the program ZIPS© (C. Coath, University of Bristol). Geochronological data are presented using the Isoplot software package (Ludwig, 2003) by

generating Tera-Wasserburg plots ($^{207}Pb/^{206}Pb$ vs. $^{238}U/^{206}Pb$) that yield discordia, and weighted average ages. Weighted average $^{207}Pb/^{206}Pb$ ages were calculated when a sample had a population of zircons that overlaps concordia. We use Tera-Wasserburg plots for ancient zircons to take advantage of the large differences in $^{207}Pb/^{206}Pb$ ratios that are not so well expressed in the conventional Wetherill Concordia plot.

3.5 Zircon trace-element geochemistry

All zircon rare earth element ($[REE]_{zirc}$) analyses reported herein were measured on the UCLA Cameca *ims*1270 ion microprobe following the approach described by Schmitt and Vazquez (2006). Analysis spots were ~25 μm in diameter and carefully positioned to overlap previous U-Pb geochronology analysis points to provide internally-consistent data sets. The REE intensities were normalized to $^{30}Si^{+}$ and corrected for interfering oxides. The trace element content of NIST standard glass 610 was used to determine the analytical sensitivity. Instrument stability was monitored by regular and frequent bracketed measurements on standard zircon 91500.

4. Results

4.1 Petrographic analysis

4.1.1. Metamorphism of Innuksuac Complex supracrustals

A suite of characteristic NSB and USB samples were earmarked for petrographic analysis; compositional descriptions of these samples are provided in the next section (4.2). Ukaliq sample

IN14032A is provisionally interpreted by us as a (mafic) matrix-hosted "meta"-conglomerate (Caro et al. 2016). Although quartz is subordinate in this rock, we interpreted it to have a conglomerate protolith based on the mineralogy and association of strongly s-deformed quartz "clasts" that are similar to samples described in the "Porpoise Cove" locality (e.g. Darling et al. 2016). Thin section studies also revealed the presence of rounded zircon grains interpreted by us to be detrital. The main mineral assemblage of this sample is anthophyllite + muscovite + quartz + rutile + zircon (**Figure 6a**). In retrogression, former biotite is now completely replaced by stilpnomelane (a common phyllosilicate in ferruginous sediments such as metagreywackes), and anthophyllite is replaced by chlorite + talc.

Sample IN12016 is a granite from the Boizard rocks. The mineral assemblage is chlorite + epidote + albite + K-feldspar + muscovite + titanite + quartz (**Figure 6b**). Chlorite + epidote + titanite replace former biotite. Muscovite + epidote also grow within albite porphyroblasts. Epidote shows different contrast values in the BSE images indicative of variable REE contents. The Ce-rich epidote (allanite) probably replaces former monazite grains (e.g. Finger et al. 1998).

Sample IN14036 is a grey gneiss collected to the west of the NSB and contains the mineral assemblage biotite + plagioclase + muscovite + quartz + zircon (**Figure 6c**). Biotite shows retrogressive replacement by the assemblage chlorite + muscovite + titanite.

Sample IN12044 is a Voizel tonalite sample and contains the mineral assemblage biotite + K-feldspar + plagioclase + quartz + apatite (**Figure 6d**). It is evident from this sample that retrogression led to the formation of the secondary assemblage chlorite + titanite + epidote replacing biotite and plagioclase. Calcite also occurs in small veins.

4.1.2. Secondary jaspilite in the Nuvvuagittuq rocks

Later hydrothermal metamorphism in parts of the NSB – exemplified in the samples described in Sec. 4.1.1. – also led to re-hydration and locally extensive formation of structurally discordant (and locally as box work veinings) jaspilite (**Supplementary Figures S2)**. This process is described in detail elsewhere for other similarly metamorphosed banded iron formations (e.g. Czaja et al. 2018). It is evident given the metamorphic history and the obvious later (discordant, post-deformation) emplacement of the jaspilites, that the alleged microfossil features claimed by Dodd et al. 2017 could not be primary to the rocks.

4.2. Whole-rock geochemistry

4.2.1. Central Tonalitic Gneiss

The largest outcrop of the Central Tonalitic Gneiss (CTG) is found near the geometric center of the NSB. Field observations show that rather than constituting a single mass of homogenous tonalitic gneiss, outcrops of the CTG instead comprise diverse interleaved granitoid gneisses and biotite-rich bodies (including possible paragneisses) with highly variable grains sizes; all are foliated in a general N-S direction (**Supplementary Figure S3**). Disrupted and strongly recrystallized enclaves of rocks that superficially resemble banded iron-formations (at least in mineralogy), which show evidence for extreme quartz mobility and schlieren are also found locally. Although difficult to assess, it is possible that this BIF was originally part of the Nuvvuagittuq supracrustal succession before becoming engulfed by these intrusive granitoids. Previous works (O'Neil et al. 2007, 2019) proposed that the CTG was genetically related to the

enclosing gneisses of the NSB (i.e. Voizel suite) but with no supportive evidence from geochronology.

The three CTG gneiss samples investigated (see sec. 4.3.1) here plot compositionally on the border between tonalite and granodiorite on the conventional TTG classification diagram (**Figure 7**; Barker, 1979). These have typical (felsic) granitoid REE patterns with chondrite-normalized LREE enrichments around 100, and HREE enrichment of about 10, although the sample collected somewhat outside the main lobe of the NSB (IN14035) is less enriched in REEs than the other more 'interior' samples (IN05001, IN12012). These latter two interior samples have weak negative Eu anomalies (0.66 and 0.95) whereas sample -035 shows a weak positive Eu anomaly (1.07; **Figure 8**). On a multi-element plot, all three show typical granitoid patterns with strong negative Nb anomalies (all have Nb/Nb* = 0.13) and moderate Ti anomalies (0.48 to 0.67). Samples IN05001 and IN14035 also have positive Zr anomalies, with values of 1.92 and 1.45, respectively (all whole-rock geochemical data are reported in **Supplementary Table S1)**.

4.2.2. Voizel suite

In outcrop, the coarse-grained Voizel (Avoi) rocks appear gray or white, depending on the degree of weathering (**Supplementary Figure S4**). They have a pronounced gneissic texture with a foliation trend that conforms to the structural outline of the NSB and USB as seen in comparative field and aerial photographs, as well as regional-scale Google-Earth images. Unlike at the NSB, the Avoi rocks disrupt and enclose the USB into 1-10 m-scale enclaves except for a few rare cases. For this study, eight Avoi samples were chosen for geochemical analysis. Three come from the upper (northern) lobe of the Ukaliq locality and within the mass of Voizel gneisses (IN12014, IN12026, and IN12027), and a further five samples come from the lower

(southern) USB lobe (IN12041, IN12044, IN12046, IN12050, and IN12056; **Figure 3**). These rocks plot in the tonalite, trondhjemite, granodiorite, and quartz monzonite fields on the TTG classification diagram (**Figure 7**). On an REE plot, the samples have typical TTG gneiss patterns, as above with the CTG. Samples IN12050 and IN12027 fall in the quartz monzonite field and have large positive Eu anomalies, with Eu/Eu* values of about 2. Samples IN12050 and IN12014 have relatively low concentrations of REE overall, and are depleted in HREE relative to other samples. Overall, Avoi samples show typical Archean igneous felsic patterns with strong negative Nb anomalies (Nb/Nb* values between 0.05 and 0.51) and moderate Ti anomalies (Ti/Ti* values between 0.28 and 0.70).

4.2.3. Boizard suite

Two samples of Boizard suite rocks were selected for analysis; the rocks are coarse grained, pink, K-feldspar-bearing, have little to no fabric (**Supplementary Figure S5**), and plot in the granite and quartz-monzonite fields (**Figure 7**). The HREE enrichments for these samples are around 10 (normalized to chondrite) and both exhibit negative Eu anomalies (Eu/Eu* values between 0.50 and 0.71). On a multi-element plot, the Aboi samples have typical Archean igneous felsic patterns with strong Nb anomalies (Nb/Nb* values between 0.29 and 0.02) and moderate Ti anomalies (Ti/Ti* values between 0.48 and 0.49). The Boizard suite dominates the landscape of the Innuksuac Complex. Its rocks enclose the Voizel suite and these in turn envelope the ancient gneisses hosting supracrustal rocks.

4.2.4. Ancient granitoid gneisses from the Ukaliq locality

In places, rare, thin (0.1-1 m-scale) variably banded gray TTG gneisses can be seen to crosscut the various amphibolitic USB enclaves in the Ukaliq locality. Field relations suggest that these gneisses pre-date the dismemberment of what was a previously a coherent supracrustal belt or belts (*sensu lato*) via extensive intrusions of Avoi granitoids accompanied by deformation (**Supplementary Figure S6**). Three of these crosscutting gneissic sheets were sampled for analysis, and all show typical Archean igneous felsic patterns with chondrite normalized LREE enrichments similar to the other gneisses described above. These samples have positive and negative Eu anomalies (Eu/Eu* values between 0.89 and 1.45). The three gneissic samples also have strong negative Nb anomalies (Nb/Nb* values between 0.14 to 0.17) and moderate Ti anomalies (Ti/Ti* values between 0.45 and 0.63).

4.2.5. Candidate volcano-sedimentary protoliths from Ukaliq

The largest, best-preserved ~50-100m rafts of Ukaliq supracrustals comprise alternating bands of variably recrystallized BIF and/or quartz±amphibole±pyroxene±magnetite rocks; massive quartzite with relict banding that may include faint cross-bedding structures, possible graded bedding and/or stretched clasts; fine grained, strongly banded amphibolitic gneisses; massive to layered ultramafic schists; and sheets or dikes of trondhjemitic gneiss (**Figure 9**). The northernmost extension of the Ukaliq supracrustal belt found in our field studies (Caro et al 2017) is represented here by a coarse-grained quartzite (sample IN14032A), the protolith of which is interpreted by us as a quartz-pebble metaconglomerate within a broad sequence of quartzitic rocks of possible detrital origin as also found in the NSB (Cates and Mojzsis, 2007, 2009; Cates et al. 2013; Dauphas et al. 2007; Darling et al. 2013).

446 *4.2.6. Sample IN14036 – an orphaned member of the CTG?*

447 This grey gneiss is similar in appearance to the CTG gneisses but comes from the west of the
448 main NSB outcrops (**Figure 3; Supplementary Figure S7**). The sample also has a positive Eu
449 anomaly (Eu/Eu* = 1.08), a strong negative anomaly (Nb/Nb* = 0.12), and a moderate Ti
450 anomaly (Ti/Ti* = 0.68). We return to this sample later, owing to the fact that the geochronology
451 revealed it to be older than the CTG gneisses.

452

453

454 **4.3 U-Pb zircon geochronology**

455

456 4.*3.1. Central Tonalitic Gneiss*

457 The three CTG samples with geochemical data were prepared for geochronological analysis.
458 Following on the previous descriptions (see sec. 4.1.1), one of these was collected from the
459 internal northwestern margin of the NSB (IN05001), another was collected from the internal
460 westernmost limit of the NSB (IN12012), while the third was collected at the external western
461 limit of the NSB (IN14035).

462 For sample IN12012 the weighted mean age ($^{207}Pb/^{206}Pb$) of the 11 most concordant grains
463 (chosen grains are within 10% of concordia) is 3652 ± 14 Ma (**Figure 10**). These zircons tend to
464 mostly be zoned cores surrounded by thin rims; the rims are too thin to measure by conventional
465 ion microprobe techniques (**Supplementary Figure S1**). Retrospective imaging of younger age
466 spots which do not plot within 10% of concordance show that they come from altered cores filled
467 with fractures. For sample IN05001, the weighted mean age of the 14 grains that cluster on the
468 concordia line is 3487 ± 15 Ma (**Figure 10**). Zircons extracted from this sample are considerably

more fractured and filled with inclusions than those of sample IN12012, but some preserve oscillatory zoning around cores. For sample IN14035, a total of 24 spots were analyzed on 24 grains. The weighted mean age of the grains that cluster on the concordia line (within 10% concordance) is 3647 ± 10 Ma (all geochronological data are reported in **Supplementary Table S2**). It is evident that samples IN12012 and IN14035, although spatially separated, have well-constrained ages that are essentially identical within error.

4.3.2. Voizel suite

Seven samples from the Voizel suite with whole-rock geochemistry data were selected for geochronology. Three samples are from the northern lobe of the USB (IN12014, IN12026, and IN12027) whereas four samples are from its the southern lobe (IN12041, IN12044, IN12046, and IN12050). Sample IN12014 gives an upper intercept age of 3550 +52 / -44 Ma (MSWD = 4.7) based on assessment of 10 analyses on 10 zircons. Two zircon grains upon which there are four analyses that were not included in the collective age determination yield a weighted mean $^{207}Pb/^{206}Pb$ age of 1871 ± 86 Ma. These grains were highly discordant but trace along a horizontal axis on the Tera-Wasserburg plot, suggestive of recent lead loss (**Figure 11**). Sample IN12026 gives an upper intercept age of 3481 ± 84 Ma (MSWD = 1.9) with a large scatter around the discordia. Sample IN12027 yields a weighted mean $^{207}Pb/^{206}Pb$ age from the four most concordant zircons of 3519 ± 16 Ma. The southern USB lobe samples have ages that overlap these within error (with a skew towards slightly older ages). Sample IN12041 has an upper intercept concordia age of 3550 ± 120 Ma (MSWD = 11.6). IN12044 has an upper intercept age of 3554 ± 46 Ma (MSWD = 1.1) from analyses that plot on

492 discordia. Sample IN12046 has an upper intercept concordia age of 3483 ± 140 Ma (MSWD =
493 11.6) from analyses that are spread around the discordia. A weighted average age of 3515 ± 140
494 Ma comes from analyses of the most concordant grains (within 3% of concordia) and are
495 typically from larger grains.

496 Sample IN12050 comes from the easternmost margin of the Voizel suite, near the contact
497 with the Boizard suite, and has an upper concordia intercept age of 3437 ± 170 Ma (MSWD =
498 17). Although there are multiple upper intercept ages of ca. 3550, no analyses from individual
499 Voizel suite zircons are this old. Instead, the oldest individual spot ages (ca. 3530) are from the
500 cores of euhedral to subhedral zircons with younger overgrowths, whereas the younger
501 population ages are exclusively from zircon rims (**Supplementary Figures S1**).

502 With regards to the high degree of scatter in some of the upper concordia intercept ages
503 reported here (with high MSWD), such values are not uncommon in polycyclic metamorposed
504 early Precambrian terranes (e.g. Corfu 2013).

505

506 *4.3.3. Boizard suite*

507 Two samples from the Boizard suite with whole-rock geochemistry were selected for
508 geochronology. One was collected to the east of the northern lobe of the USB (IN12016), and
509 one was taken to the south of the lower lobe (IN12054; **Figure 3**). Sample IN12016 has a
510 weighted mean $^{207}Pb/^{206}Pb$ age of 2706 ± 19 Ma from a total of 6 grains that cluster on or close
511 to concordia (**Figure 12**). Several old domains – as cores surrounded by zoned igneous
512 overgrowths – were recognized from zircons within this sample with $^{207}Pb/^{206}Pb$ dates up to ca.
513 3700 Ma; **Supplementary Figures S1, Supplementary Table S1**). Other zircons with dates
514 older than 3000 Ma also come from core regions of the grains, although in images some of these

appear altered and fractured. Young, highly discordant dates come from zircons with altered cores that appear to be either metamict or filled with fractures and inclusions. Four highly discordant zircon grains give a weighted mean $^{207}Pb/^{206}Pb$ age of 1175 ± 340 Ma, but these trace along a horizontal axis on the Tera-Wasserburg plot, suggestive of recent lead loss and should be considered estimates. Sample IN12054 has a weighted mean $^{207}Pb/^{206}Pb$ age of 2720 ± 20 Ma from a total of 8 analyses that cluster on or near concordia. The oldest date (and not, therefore necessarily age) in this sample, 3431 ± 6 Ma, comes from a grain with a core surrounded by a younger rim (2921 ± 9 Ma). We find that the grains from the younger but still concordant population have euhedral to anhedral habits.

4.3.4. Structurally intrusive gneisses to the Ukaliq supracrustal belt enclaves

Four samples collected from structurally invasive gneisses transecting enclaves within the various USB sites were selected for geochronology. Two of these were taken from the northern lobe (IN12017 and IN12031) and two were taken from the southern lobe (IN12042 and IN12053). Sample IN12017 gives a concordia upper intercept $^{207}Pb/^{206}Pb$ date (not necessarily 'age') of 3598 +44 / -37 Ma, owing to the fact that the majority of analyses come from discordant zircons (**Figure 13**). Some of the younger, discordant zircons in this sample have complex textures typical of hydrothermal growth or metamictization (Corfu et al. 2003) whereas the oldest zircon in this sample (3653 ± 8 Ma) comes from a core with a thick, zoned overgrowth (**Supplementary Figures S1**). Sample IN12031 has two populations, with the older population more concordant which yields a weighted mean $^{207}Pb/^{206}Pb$ age of 3505 ± 5 Ma. The younger population lies on the discordia with the older population with an upper intercept at 3496 ± 35 Ma. Sample IN12042 also gives an upper intercept at 3492 ± 190 Ma from a cluster of the most

concordant grains, but the oldest analysis in this sample comes from a 30% discordant grain with a $^{207}Pb/^{206}Pb$ date of 3694 ± 9 Ma. Sample IN12053 seems to have three populations, all of which are discordant. The youngest, most discordant grains yield a weighted average $^{207}Pb/^{206}Pb$ date of 2292 ± 120 Ma and come from either zircon rims or metamict cores (**Supplementary Figures S1**). One spot on a zircon with 25% concordance gave a weighted average $^{207}Pb/^{206}Pb$ date of 3362 ± 19 Ma. The oldest population comprises two grains with $^{207}Pb/^{206}Pb$ ages of 3582 ± 9 Ma and 3694 ± 19 Ma (**Supplementary Table S1**). These grains are euhedral to subhedral, and the oldest age domains correspond to zircon core surrounded by rims that have spongy textures typical of hydrothermal alteration (e.g., Hoskin and Schaltegger, 2003).

4.3.5. Igneous and sedimentary protoliths in the Ukaliq supracrustal belt enclaves

A quartz-biotite schist sample IN14032A interpreted to be a 'meta-conglomerate' based on field relations, petrology (see sec. 4.2) and resemblance to other rocks from the Porpoise Cove locality of the NSB (e.g., Cates et al. 2013), was discovered in the upper lobe of the Ukaliq belt. This rock is within a succession of quartzites, amphibolites, and ultramafic rocks (**Figure 8d;** Caro et al. 2017) surrounded by Voizel gneisses. This sample has several different zircon populations the oldest of which is interpreted here to be of detrital origin (see sec. 5.3); the oldest of these clusters around a weighted average $^{207}Pb/^{206}Pb$ age of 3736 ± 5 Ma (**Figure 13**). Younger, smaller, populations cluster around ca. 3650 Ma and ca. 2700 Ma. It is important to note that these zircon U-Pb age populations are defined by spot analyses with less than 5% discordance. This sample has a group of highly reversely discordant grains, with ages between 3185 ± 28 Ma and 3440 ± 29 Ma.

561 *4.3.6. Granitoid gneiss sample IN14036 from outside the NSB*

562 Gray gneiss sample -036 was collected to the west of the westernmost limb of the NSB
563 (**Supplementary Figure S7**), approximately 150 m west of the outcrop of possible CTG-related
564 sample IN14035 (**Figure 3**). Sample -036 is similar in appearance to other TTGs analyzed herein
565 (in particular samples IN12012 and IN12044), but yields a much older age. It has an upper
566 concordia intercept $^{207}Pb/^{206}Pb$ age of 3760 ± 17 Ma, with a weighted mean age, comprising only
567 the least discordant grains, of 3750 ± 7 Ma. Zircons extracted from this sample generally plot on
568 concordia, with only a few analyses defining the discordia (**Figure 13**).

569

570 **4.4 Zircon Trace-element Geochemistry**

571

572 A routinely used means to determine whether a particular zircon age population is original to
573 its host rock (e.g. Manning et al. 2006; Cates and Mojzsis, 2009; Cates et al. 2013; Mojzsis et al.
574 2014; Reimink et al. 2014), is the lattice strain model for ionic compatibility between the
575 composition of a mineral (in this case, zircon) and a melt of the composition of the host rock
576 (Blundy and Wood, 1994; Taylor et al. 2015). In those rocks with multiple zircon age
577 populations, application of this model can help to determine the most likely age of the rock under
578 the assumption that the original melt and native, age-representative zircons, formed in
579 equilibrium. The assumption requires that the composition of the rock hosting the minerals in
580 question represents the last melt composition (Onuma et al. 1968). As described elsewhere
581 (Taylor et al. 2015) the model takes advantage of the chemical similarities of the trivalent rare
582 earth elements, where the main controlling factor for how easily these ions are incorporated into
583 growing minerals is the predictable change in ionic radius with increasing atomic number from

584 the lanthanide contraction. It has long been known that HREEs are more compatible in zircon
585 than LREE because their ionic radii approach that of Zr^{4+} (0.84 Å in eight-fold coordination).
586 Thus, the distribution of REEs in zircon is controlled by the composition of the melt, and the
587 REE_{Zr}/REE_{rock} should plot as a parabola for a zircon that crystallized in a melt with the
588 composition of the whole rock representative of that melt (e.g. Trail et al. 2007; Mojzsis et al.
589 2014 and references therein).

590 Partition coefficients were determined for each zircon in our database (REE_{zirc}/REE_{WR}) and
591 fitted using the Blundy and Wood (1994) lattice strain model. The best fit parabola (described by
592 its R^2 value) for the exponential function was then calculated iteratively over 1000 model fits to
593 the data. The higher the R^2 value, the better the model fit of the data to the lattice strain model
594 and consequently the more likely it is that the zircon REE chemistry comports with the whole-
595 rock composition. In this work, we selected a subset of concordant zircons from the Voizel suite
596 and CTG granite-granitoid gneisses for REE analysis (results in **Figure 14a;** data reported in
597 **Supplementary Table S3**) and lattice-strain modeling in order to refine our estimate(s) of the
598 most likely crystallization age(s) for these two units. Three concordant zircons from the Voizel
599 rocks (IN12027 and IN12046) and four concordant zircons from CTG sample IN12012 and one
600 from IN05001 were set aside for REE analyses. The results of our analysis show that only the
601 oldest zircons in this particular analysis have statistically good fits ($R^2 \geq 0.9$) with their host-rock
602 REE compositions (**Figure 14b**), which we interpret to represent the crystallization age.
603
604 **4.5 Zr-in-rutile geothermometry**
605

606 The temperature dependence of Zr incorporation into rutile grown in equilibrium with quartz
607 and zircon yields a widely useful single-mineral geothermometer (Zack et al. 2004; Watson et
608 al. 2006; Tomkins et al. 2007). Petrography of the four samples selected for Zr-in-rutile
609 geothermometry (Sec. 4.2) revealed an older high-grade mineral assemblage and a texturally
610 later secondary mineral assemblage as previously shown in **Figure 6**. Owing to the pervasive
611 retrogression of the samples (complete replacement of biotite, plagioclase) it was not possible to
612 constrain P-T conditions using phase equilibrium calculations; instead this geothermometer
613 provides a constraint on temperature (T) by analyzing rutiles from the purported
614 metaconglomerate sample IN14032A. A total of 41 rutile analyses were performed by electron
615 microprobe at the Institute of Mineralogy and Petrography, University of Innsbruck (Austria); Zr
616 contents range from 407 ppm to 914 ppm (**Supplementary Table S4**). No differences between
617 core and rim analyses were found. The calibration of Tomkins et al. (2007) yielded T of 660-
618 730°C at 0.6 GPa and calculated mean T is 670°C ± 40°C (2σ). Due to the lack of precise
619 pressure (P) constraints an arbitrary P of 0.6 GPa was chosen, which is in agreement with the
620 observed mineral assemblage in sample IN14032A. The calculations also show that P has only
621 minor influence on the estimates presented here since mean T varies only from 660°C at 0.4 GPa
622 to 680°C at 1 GPa (Triebold et al. 2012). We find that these results are in good agreement with
623 the earlier study of Cates and Mojzsis (2009) for the NSB rocks, which used the conventional
624 garnet–biotite and plagioclase–hornblende geothermometry.
625
626 **4.6 Rutile crystal chemistry as provenance indicator**
627
628 Geochemical discrimination studies of specific detrital minerals can be used in provenance

629 characterization. The widespread occurrence of rutile in medium to high-grade metamorphic
630 rocks as well as sedimentary rocks, and its high mechanical and chemical stability during
631 weathering, transport and diagenesis make rutile a prime-candidate for such work (Triebold et al.
632 2012). It was shown that Cr and Nb abundances can effectively be used to distinguish between
633 metamorphosed mafic and pelitic lithologies; Fe content also serves as an indicator of
634 metamorphic origin since metamorphic rutile contains generally >1000 ppm Fe (Zack et al.
635 2004). Rutiles investigated in this study have Cr contents ranging from 300 to 2400 ppm and Nb
636 contents ranging from 570 to 1900 ppm. It is also noteworthy that Fe contents range from 300 to
637 3900 ppm, and most analyses exceed 1000 ppm. According to the chemical classification of
638 Triebold et al. (2012) most of our rutile analyses suggest a metapelitic origin with only 7 rutile
639 analyses indicative of origin from metamorphism in the mafic rock.
640
641 **5. Discussion**
642
643 *5.1. Geology, age and origin of Voizel suite and Central Tonalitic gneisses*
644 Although long considered part of the same suite, new evidence shows that the Voizel and
645 CTG instead belong to separate generations of TTG gneisses within the Inukjuak Domain. Their
646 geochemical properties are similar: all the felsic gneisses analyzed here yield multi-element plot
647 patterns that conform with classic Archean continental crust signatures and have negative Nb and
648 Ti anomalies (**Figure 8b**; Rudnick, 1995). Both units are primarily tonalitic gneisses with about
649 70 wt.% SiO_2 and moderate concentrations of alkalis ($NaO+CaO+K_2O$ ~ 9.0 wt.%). The Voizel
650 suite rocks, however, are more depleted in REEs (particularly the HREEs) than those from the
651 CTG, and two Voizel suite rocks that plot in the quartz monzonite field as opposed to the tonalite

652 field (**Figure 7**) also have positive Eu anomalies. Gneissic rocks with these types of features
653 (low REE concentrations, positive Eu anomalies) in ancient (Hadean-Archean and younger)
654 metamorphic terranes have been interpreted as leucosomes during migmatite formation (e.g.
655 Sawyer, 2008; Cates et al. 2013; Mojzsis et al. 2014). Although these small geochemical
656 differences could be the result of internal variability, our preferred interpretation is that the
657 geochronological differences between these two suites point to two distinct emplacement events.
658 The Voizel suite is ca. 3550 Ma old based on upper concordia intercept ages, even if it has no
659 individual zircon analysis with an age above 3538 ± 6 Ma (IN12046). The zircon with the best fit
660 for the lattice strain model is among the oldest of the zircons (Sec. 4.4), with an age of 3530 Ma
661 and 99% concordant (IN12027). In contrast to the Voizel suite samples, the CTG sample
662 IN12012 has abundant zircons with ages up to 3663 ± 5 Ma, and the zircon with the best fit for
663 the lattice strain model is 3661 ± 8 Ma. The ca. 3660 Ma cores are consistent with igneous
664 growth and are interpreted as the maximum age of the CTG. Thus, the age of the CTG as
665 determined by the upper intercept of the discordia on the Tera-Wasserburg plot, is the age of
666 sample IN12012, which is 3652 ± 14 Ma. This age is about 100 million years older than the
667 previously (albeit provisionally) assigned values for the Voizel suite (O'Neil et al. 2007, 2019
668 and references therein). Furthermore, David et al. (2009) presented geochronological data for a
669 single mylonitized sample from the northwest of the margin of the NSB, which was resampled
670 by us as IN14035, and our data are in agreement. As IN14035 gives a weighted mean $^{207}Pb/^{206}Pb$
671 zircon age of ca. 3650, this rock is most likely related to the CTG rather than to the more widely
672 distributed and volumetrically more important Voizel suite.
673
674 *5.2. Nature of the Boizard suite gneisses*

675 We find that the Boizard suite is both geochemically and geochronologically distinct from
676 the other granitoid gneisses described within the Inukjuak Domain. It is a meta-granite and lacks
677 the foliation observed in the Voizel and CTG outcrops. Zircons from the Boizard suite cluster
678 mostly around ca. 2700 Ma, with some degree of inheritance. These older, inherited ages all
679 come from grains with rounded cores, some of which are surrounded by igneous rims with strong
680 oscillatory zoning. The inherited cores of the Boizard suite zircons include ages previously seen
681 in the NSB (Cates et al. 2013), which suggests that the granites were extensively contaminated
682 by zircons from the supracrustals during emplacement.
683
684
685 *5.3. Candidate Innuksuac Complex supracrustal rocks beyond the NSB*
686 In contrast with the Nuvvuagittuq outcrops, the Ukaliq rocks are more strongly deformed into
687 a set of relatively small disconnected mafic to ultramafic enclaves with very minor (<1% of total
688 outcrop) metasedimentary components. The three TTG gneisses sampled for this study were
689 selected because they were mapped to cross-cut USB amphibolites. Results of our U-Pb zircon
690 geochronology show that they are generally younger than those found in the ca. 3780 Ma
691 Nuvvuagittuq outcrops further to the southwest (Cates and Mojzsis, 2007). Zircons from the
692 oldest Ukaliq supracrustal belt enclave samples mostly yield an upper intercept age of ca. 3600
693 Ma (sample IN12017, **Figure 13**), although the oldest and still highly concordant individual
694 grain in this particular sample is ca. 3650 Ma. These ages might be interpreted as evidence that
695 modification and dismemberment of the USB was contemporaneous with the emplacement of the
696 CTG. Associated granitoid gneisses, which preserve the oldest age in this sample is tonalitic with
697 less than 200 ppm Zr (**Supplementary Table S1**), thus making inheritance an unlikely source of

698 the oldest grains. The other two supracrustal gneiss samples are granodioritic. Sample IN12053,
699 with a zircon population of ca. 3360 Ma also has two older grains at ca. 3700 Ma and ca. 3580
700 Ma, but these grains are discordant (~30%). This sample has low Zr concentration (111 ppm),
701 again arguing against inheritance, and all of these analyses come from zircon cores with
702 oscillatory zoning. Thus an absolute age of this unit cannot be established, though the older
703 analyses likely best represent the sample. Sample IN12053 also has a population of ca. 2700 Ma
704 zircons, which is unsurprising due to the proximity of the enclave to the contact between the
705 Voizel suite and Boizard suite. This age has not been observed in any of the other enclave
706 samples analyzed in this study.

707 The quartz-biotite schist we provisionally assigned as a quartz-pebble "metaconglomerate"
708 sample IN14032A has a minimum age of formation of 3550 Ma, as determined by field
709 relationships with the surrounding Voizel suite. If the different disrupted USB rafts are related to
710 one another, then the oldest age of the felsic enclaves sets the minimum age at 3600 Ma. The
711 oldest zircon in this sample, at 3771 Ma, if interpreted as such gives a minimum age of the
712 detrital source material (**Supplementary Table S2**; **Figure 13**). A small zircon population in this
713 sample the same age of the CTG further supports the idea that the dismemberment of the USB
714 commenced at 3650 Ma, which led to partial re-setting of the ca. 3770 Ma zircons (Cates and
715 Mojzsis, 2009; Cates et al. 2013). This could also suggest that the USB incorporated detritus
716 after the emplacement of the CTG, but not since that time, and instead the quartz-biotite schist
717 has a maximum age of 3650 Ma

718 Sample IN14036 was collected outside of the limits of the NSB. However, since its age of ca.
719 3760 is the same as other samples collected from the NSB (Cates and Mojzsis, 2007; Cates et al.
720 2013), it is likely related to the supracrustals in some way. This particular sample could represent

721 an enclave of the NSB within the surrounding TTGs, suggesting that the NSB is not as cohesive
722 as previously thought, or that the section of CTG that separates this sample from the rest of the
723 belt is intruding the NSB, which extends further west than previously thought. It is also possible
724 that the USB exists as a set of enclaves within the Voizel, and this sample represents the
725 westernmost expression of the USB as well as a maximum age for the supracrustals. Further field
726 studies to document further Eoarchean rocks in the northern Inukjuak Domain are needed to
727 distinguish between these possibilities.
728
729
730 **6. Conclusions**
731
732 Poly-metamorphosed TTG gneisses of the Inukjuak domain were emplaced over multiple
733 generations spanning a billion years. Our results from detailed U-Pb zircon geochronology of
734 samples from both the Nuvvuagittuq and Ukaliq supracrustal belts reveal multiple generations of
735 zircon growth, spanning from ca. 3780 to 2700 Ma. These intrusive events, distributed over
736 space and time, disrupted, deformed and metamorphosed the various supracrustal enclaves of the
737 Innuksuac Complex and are recorded as episodes of metamorphic zircon growth from samples
738 collected from within the enclaves as well as in the oldest TTG gneisses (Cates and Mojzsis,
739 2007; Cates et al. 2013; cf. Darling et al. 2013).
740
741 The results of our study can be summarized as follows:
742

1. Lattice strain partition modeling differentiates between different zircon age populations based on compositional parameters, and suggests both crystallization ages and neoform zircon growth events for many of the studied units. Based on this combined approach, the age of the CTG can now be resolved to ca. 3650 Ma. The previously undated Voizel suite is about 100 million years younger, with a maximum age of approximately 3550 Ma. The Boizard suite, emplaced at ca. 2700 Ma, experienced widespread xenocrystic contamination during its emplacement and carries inherited zircons from all older suites in the terrane, including those from the NSB. Disruption and partial structural dismemberment of the Ukaliq supracrustal belt (with a maximum age of ca. 3770 Ma) may be contemporaneous to the timing of the formation of the CTG. This age relationship may provide a link to the neighboring ca. 3750-3780 Ma NSB (Cates and Mojzsis, 2007; Cates et al. 2013). Sample IN14036 represents a new expression of an old TTG gneiss to the north and west, but further field study is needed to determine whether it represents an outcrop of the NSB or USB, or something else entirely.

2. Petrological investigations of select samples show pervasive retrograde metamorphism of the mineral assemblages. Our new Zr-in-rutile thermobarometry results underscore the history of amphibolite to greenschist facies metamorphism that accompanied polyphase deformation events throughout the southern Inukjuak region. It is apparent that none of the Eoarchean Innuksuac supracrustal rocks escaped a variable history of retrograde metamorphism and deformation.

3. No confirmed microfossils older than about 3500 Ma exist, probably because all known Eoarchean rocks of sedimentary protolith – including those of the Inukjuak Domain – are both metamorphosed, deformed and variably recrystallized. In our view, the claims of Dodd et al. 2017 that microfossil shapes including "hematite tubes and filaments" are found in secondary jaspilite veins from Nuvvuagittuq are no exception. Indeed, many of the structures they describe including associations of hematite, quartz and magnetite are documented as non-biological features (e.g. Figueiredo et al. 2008). The geologic history described herein precludes preservation of any fine-scale primary structural features, either "stromatolites" or purported fragile microfossil shapes hosted in jaspilite box-work veinings (Taylor 2011). Despite such shortcomings, the Inukjuak Domain supracrustal rocks are a unique complementary repository to the only other large (~3000 km^2) domain of Eoarchean rocks known, those of the Itsaq Gneiss Complex in West Greenland. Investigations of the Innukjuak Domain have only scratched the surface of a region that was nots recognized for its enormous antiquity until recently (2001-2002). To date, the most exciting rocks reported from the Inukjuak region are those that are also easily accessible by boat, but otherwise the vast inland localities can only be spot-checked here and there, with many more apparent from aerial photographs and satellite images.

4. That some rocks from the area indeed include paragneisses with protoliths ascribable to detrital "quartzites" and "conglomerates" means that they could preserve one of the oldest if not the oldest unconformities thus far recognized. For instance, quartz-rich sedimentary rocks appear to overly ca. 3650 Ma TTG basement in several places in the Nuvvuagittuq and Ukaliq outcrops. Also, although data reported herein are largely of a

reconnaissance nature on a rather extensive and well-selected suite of "reconnaissance samples" it is striking to note that there are no zircon grains older than about 3800 Ma despite thousands of zircon analyses since 2005. This result in of itself casts serious doubts on the interpretation that the Inukjuak Domain, including the Nuvvuagittuq Supracrustal Belt, preserves a formational history that goes back half a billion years older (to ca. 4300 Ma; cf. O'Neil et al. 2007, 2019).

5. The ca. 3.8 Ga Innuksuac Complex provides a hitherto unexpected windfall in the study of early Earth materials by providing a new, more global perspective beyond that of the Isua, Akilia, Manfred and Saglek Harbor rocks. The ~12,000 km^2 Inukjuak Domain is unquestionably an important resource that adds to our understanding of the physical, chemical, (proto-)biological and geodynamical state of the Earth's surface at the Hadean-Eoarchean transition around 3850-3800 million years ago.

(8535 words)

Acknowledgements

J.G. thanks the Department of Geological Sciences at the University of Colorado for financial support during the preparation of this work. S.J.M. gratefully acknowledges logistical assistance for work in the Nuvvuagittuq area from the Pituvik Corporation of Nunavik (Québec), and in particular to the indispensable assistance and advice provided by General Manager Mr. Mike Carroll. The NASA Exobiology Program (Grant 09-EXOB09-0123, NNH09ZDA001N-EXOB Investigating the Hadean Earth) supported this work from 2009 to 2012. Subsequently, from 2015-2018 our study was funded by the Collaborative for Research in Origins (CRiO) supported by The John Templeton Foundation (principal investigator: Steven Benner/FfAME): the opinions expressed in this publication are those of the authors, and do not necessarily reflect the views of the John Templeton Foundation. S.J.M. also extends a special thanks the University of Lorraine and CNRS-CRPG (Nancy, France) for a Visiting Professor appointment in June 2019 wherein

this manuscript was completed. G.C. acknowledges financial support from the Agence Nationale de la Recherche (Grant ANR-11-JS56-0012 “DESIR”). We thank Elizabeth Bell, Fannie Thibon, Sarah Davey, Martin Guitreau, Jonathan Oulton, Antoine Roth and Dustin Trail for valuable discussions and assistance in the course of fieldwork. Detailed and constructive comments by A.P. Nutman and an anonymous review improved this work. Correspondence and request for materials should be addressed to S.J.M. (mojzsis@colorado.edu)

REFERENCES CITED

Anders E., Grevesse N., 1989. Abundances of the elements- meteoric and solar. Geochimica et Cosmochimica Acta 53, 197-214.

Barker, F., 1979. Trondhjemite: definition, environment and hypothesis of origin. In: F. Barker (Ed.), Trondhjemites, Dacites and Related Rocks. Elsevier, Amsterdam, 1–12.

Bell, E.A., Boehnke, P., Harrison, T.M., 2017. Applications of biotite inclusion composition to zircon provenance determination. Earth and Planetary Science Letters 473, 237-246.

Bell, E.A., Boehnke, P., Harrison, T.M., Wielicki, M.M., 2018. Mineral inclusion assemblage and detrital zircon provenance. Chemical Geology 477, 151-160.

Berclaz, A., Godin, L., david, J., Maurice, C., Parent, M., Francis, D., Stevenson, R., Leclair, A. 2003. Géologie de la Ceinture de Nuvvuagittuq (env. 3,8 Ga), Nord-Est de la Province du Supérieur : vers une approche multidisciplinaire. *Dans* : Résumé des conférences et des photoprésentations, Québec Exploration 2003. Ministère des Ressources naturelles, de la Faune et des Parcs, Québec; DV 2003-09, page 50.

Black L.P., Kamo, S.L., Williams I.S., Mundil R., Davis D.W., Korsch R.J., Foundoulis C., 2003. The application of SHRIMP to Phanerozoic geochronology; a critical appraisal of four zircon standards. Chemical Geology 200, 171–188

Bleeker, W., 2002. Archaean tectonics: a review, with illustrations from the Slave craton. *In*, Fowler, C. M. R., Ebinger, C. J. and Hawkesworth, C. J. (eds) The Early Earth: Physical, Chemical and Biological Development. Geological Society, London, Special Publications, 199, 151-181. 0305.

Blundy J., Wood B., 1994. Prediction of crystal-melt partition coefficients from elastic moduli. Nature 372, 452-454.

877 Bridgwater, D., Allaart, J.H., Schopf, J.W., Klein, C., Walter, E.S. Barghoorn, E.S., Strother,
878 P.K., Knoll, A.H., Gorman, B.E. 1981. Microfossil-like objects from the Archaean of Greenland:
879 A cautionary note. Nature 289, 51-53.
880
881 Caro, G., Morino, P., Mojzsis, S.J., Cates, N.L., Bleeker, W. 2016. Sluggish Hadean
882 geodynamics: Evidence from coupled ^{146,147}Sm-^{142,143}Nd systematics in Eoarchean supracrustal
883 rocks of the Inukjuak domain (Québec). Earth and Planetary Science Letters 457:23-37.
884
885 Cates, N.L. and Mojzsis, S.J. 2006. Chemical and isotopic evidence for widespread Eoarchean
886 (>3700 Ma) metasedimentary enclaves in southern West Greenland. Geochimica et
887 Cosmochimica Acta 70, 4229-4257.
888
889 Cates N.L., Mojzsis S.J., 2007. Pre-3750 Ma supracrustal rocks from the Nuvvuagittuq
890 supracrustal belt, northern Québec. Earth and Planetary Science Letters 255, 9–21.
891
892 Cates N.L., Mojzsis S.J., 2009. Metamorphic zircon, trace elements and Neoarchean
893 metamorphism in the ca. 3.75 Ga Nuvvuagittuq supracrustal belt, Québec (Canada).
894 Chemical Geology 261, 98–113.
895
896 Cates N.L., Ziegler K., Schmitt A.K., Mojzsis S.J., 2013. Reduced, reused and recycled: Detrital
897 zircons define a maximum age for the Eoarchean (ca. 3750-3780 Ma) Nuvvuagittuq Supracrustal
898 Belt, Québec (Canada). Earth and Planetary Science Letters 362, 283-293.
899

Corfu, F., 2013. A century of U-Pb geochronology: The long quest towards concordance. Geological Society of America Bulletin 125, 33–47.

Corfu F., Hanchar J.M., Hoskin P.W.O., Kinny P., 2003. Atlas of zircon textures. Rev. Mineral. Geochem. 53, 469–500.

Czaja, A.D., Van Krandendonk, M.J., Beard, B.L., Johnson, C.M., 2018. A multistage origin for Neoarchean layered hematite-magnetite iron formation from the Weld Range, Yilgarn Craton, Western Australia. Chemical Geology 488, 125-137.

Darling, J.R., Moser, D.E., Heaman, L.M., Davis, W.J., O'Neil, J., Carlson, R., 2013. Eoarchean to Neoarchean evolution of the Nuvvuagittuq Supracrustal belt: New insights from U-Pb zircon geochronology. American Journal of Science 313, 844-876.

David, J., Stevenson, R.K., Nadeau, P., Godin, L., 2002. La séquence supracrustale de Porpoise Cove, région d'Inukjuak: un exemple unique de croûte paléo-archéenne (ca. 3.8 Ga) dans la Province du Supérieur. In: L'exploration minérale au Québec, notre savoir, vos découvertes. Ministère des Ressources Naturelles, Québec. DV 2002, 17.

David J., Godin L., Stevenson R., O'Neil J., Francis D., 2009. U–Pb ages (3·8–2·7 Ga) and Nd isotope data from the newly identified Eoarchean Nuvvuagittuq supracrustal belt, Superior Craton, Canada. Geological Society of America Bulletin 121, 150-163.

de Witt M., Ashwal L.D., 1997. Greenstone belts. Oxford Monographs on Geology and Geophysics 35.

Figueiredo, E.S.R.C., Lobato, L.M., Rosière, Hagemann, S., Zucchetti, M., Baars, F.J., Morais, R., Andrade, I., 2008. A hydrothermal origin for the jaspilite-hosted, giant Serra Norte iron ore deposits in the Carajás Mineral Province, Pará State, Brazil. *In* Reviews in Economic Geology 15, doi.org/10.5382/Rev.15.10

Finger, F., Broska, I., Roberts, M.P., Schermaier, A., 1998. Replacement of primary monazite by apatite-allanite-epidote coronas in an amphibolite facies granite gneiss from the Eastern Alps. American Mineralogist 83, 248–258.

Frank, E.A., Maier, W.D. and Mojzsis, S.J. (2016) Highly siderophile element abundances in Eoarchean komatiite and basalt protoliths. Contributions to Mineralogy and Petrology 171, 29.

Hoskin P.W.O., Schaltegger U., 2003. The composition of zircon and igneous metamorphic petrogenesis. Reviews in Mineralogy and Geochemistry 53, 27–62.

Kinny, P.D., Williams, I.S., Froude, D.O., Ireland, T.R., Compston, W. 1988. Early Archaean zircon ages from orthogneisses and anorthosites at Mount Narryer, Western Australia. Precambrian Research 38, 325-341.

945 Ludwig, K.R., 2003. User's Manual for Isoplot/Ex: A Geochronological Toolkit for Microsoft
946 Excel, Berkley Geochronological Center Special Publication.
947
948 Manning C.E., Mojzsis S.J., Harrison, T.M., 2006. Geology, age and origin of supracrustal rocks,
949 Akilia, Greenland. Am. J. Sci. 306, 303-366.
950
951 McDonough W.F., 1992. Composition of the primitive mantle, depleted mantle and other mantle
952 reservoirs. Int. Geol. Congr. 29, A175
953
954 McGregor, V. R., and Mason, B., 1977. Petrogenesis and geochemistry of metabasaltic and
955 metasedimentary enclaves in the Amîtsoq gneisses, West Greenland: American Mineralogist, v.
956 62, p. 887–904.
957
958 Mloszewska, A.M., Mojzsis, S.J., Pecoits, E., Papineau, D., Dauphas, N. and Konhauser, K.O.
959 (2013) Chemical sedimentary protoliths of the >3.75 Ga Nuvvuagittuq Supracrustal Belt
960 (Quebec, Canada). Gondwana Research 23, 574-594.
961
962 Nutman, A.P., McGregor, V.R., Shiraishi, K., Friend, C.R.L., Bennett, V.C., Kinny, P.D. (2002)
963 ≥3850 Ma BIF and mafic inclusions in the early Archaean Itsaq Gneiss Complex around Akilia,
964 southern West Greenland? The difficulties of precise dating of zircon-free protoliths in
965 migmatites. Precambrian Research 117, 185-224.
966

967 Nutman, A.P., Bennett, V.C., Friend, C.R.L., Horie, K., Hidaka, H. 2007. ~3,850 Ma tonalities in
968 the Nuuk region, Greenland: geochemistry and their reworking within an Eoarchaean gneiss
969 complex. Contributions to Mineralogy and Petrology 154, 385-408.
970
971 O'Neil J., Maurice C., Stevenson R.K., Larocque J., Cloquet C., David J., Francis D., 2007. The
972 geology of the 3·8 Ga Nuvvuagittuk (Porpoise Cove) Greenstone Belt, northern Superior
973 Province, Canada. In: Kranendonk M.J., Smithies R.H., Bennett V.C., editors. Earth's Oldest
974 Rocks. Elsevier, Amsterdam, pp. 219-250.
975
976 O'Neil J., Carlson R.W., Francis D., Stevenson R.K., 2008. Neodymium-142 evidence for
977 Hadean mafic crust. Science 321, 1828-1831.
978
979 O'Neil J., Francis D., Paquette J., Carlson R.W., 2012. Formation age and metamorphic history
980 of the Nuvvuagittuq Greenstone Belt. Precambrian Research 220, 23-44.
981
982 O'Neil, J., Carlson, R.W., Papineau, D., Levine, Y.E., Francis, D., 2019. Chapter 16: The
983 Nuvvuagittuq Greenstone Belt: A Glimpse of Earth's Earliest Crust in Earth's Oldest Rocks
984 (Second Edition), p. 349-374.
985
986 Onuma, N., Higuchi, H., Wakita, H., Nagasawa, H., 1968. Trace element partition between two
987 pyroxenes and the host lava. Earth and Planetary Science Letters 5, 47-51.
988

Paces J.B., Miller J.D., 1993. Precise U-Pb ages of Duluth Complex and related mafic intrusions, northeastern Minnesota - Geochronological insights to physical, petrogenic, paleomagnetic, and tectonomagmatic processes associated with the 1.1 Ga Midcontinent Rift system. Journal of Geophysical Research, Solid Earth 98, 13997-14013.

Roth A.S.G., Bourdon B., Mojzsis S.J., Touboul M., Sprung P. Guitreau M. Blichert-Toft J., 2013. Inherited ^{142}Nd anomalies in Eoarchean protoliths. Earth and Planetary Science Letters 361, 50-57.

Rudnick R.L., Fountain D.M., 1995. Nature and composition of the continental crust: A lower crustal perspective. Reviews of Geophysics 33, 267-310.

Sawyer E.W., 2008. Atlas of Migmatites. The Canadian Mineralogist, Special Publication 9. NRC Research Press, Ottawa, 371.

Schiøtte, L., Compston, W., Bridgwater, D. 1989. U-Th-Pb ages of single zircons in Archaean supracrustals from Nain Province, Labrador, Canada. Canadian Journal of Earth Sciences 26, 2636-2644.

Schidlowski, M. 1988. A 3,800-million-year isotope record of carbon in sedimentary rocks. Nature 333, 313-318.

1011 Schmitt A.K., Vazquez J.A., 2006. Alteration and remelting of nascent oceanic crust during
1012 continental rupture: Evidence from zircon geochemistry of rhyolites and xenoliths from the
1013 Salton Trough, California. Earth and Planetary Science Letters 252, 260-274.
1014
1015 Schuhmacher M., de Chambost E., McKeegan K.D., Harrison T.M., Migeon H., 1994. Dating of
1016 zircon with the CAMECA IMS 1270. In: Benninghoven A., Nihei Y., Shimizu R., Werner H.W.
1017 (Eds.), Secondaray Ion Mass Spectrometry SIMS IX. John Wiley & Sons, New York, pp. 912–
1018 922.
1019
1020 Simard M., Parent M., David J., Sharma K.N.M., 2003. Géologie de la région de la rivière
1021 Innuksuac (34K et 34L). Ministère des Ressources naturelles, RG, Québec, 2002–10.
1022
1023 Stevenson R., Bizzarro M., 2005. Hf and Nd isotope evolution of lithologies from the 3.8 Ga
1024 Nuvvuagittuq Sequence, northern Superior Province, Canada. Geochimica Cosmochimica Acta
1025 69, A391.
1026
1027
1028 Taylor, R., 2011. Boxworks and related features. In: Gossans and Leached Cappings. Springer,
1029 Berlin, Heidelberg.
1030
1031 Taylor, R.J.M., Harley, S.L., Hinton, R.W., Elphick, S., Clark, C., Kelly, N.M. 2015.
1032 Experimental determination of REE partition coefficients between zircon, garnet and melt: a key
1033 to understanding high-T crustal processes. Journal of metamorphic Geology 33, 231–248.

Trail, D., Mojzsis, S.J., Harrison, T.M., Schmitt, A.K., Watson, E.B. and Young, E.D. (2007) Constraints on Hadean protoliths from oxygen isotopes and Ti-thermometry Geochemistry, Geophysics, Geosystems 8. doi:10.1029/2006GC001449.

Touboul, M., Liu, J., O'Neil, J., Puchtel, I.S., Walker, R.J. 2014. New insights into the Hadean mantle revealed by 182W and highly siderophile element abundances of supracrustal rocks from the Nuvvuagittuq Greenstone Belt, Quebec, Canada. Chemical Geology 383, 63-75.

Triebold, S., von Eynatten, H., Zack, T., 2012. A recipe for the use of rutile in sedimentary provenance analysis. Sed. Geol., 282, 268–275.

Tomkins, H.S., Powell, R., Ellis, D.J., 2007. The pressure dependence of the zirconium-in-rutile-thermometer. J. Metam. Geol., 25, 703–713.

Watson E.B., Harrison T.M., 1983. Zircon saturation revisited: temperature and composition effects in a cariety of crustal magma types. Earth and Planetary Science Letters 64, 295-304.

Watson, E.B., Wark, D.A., Thomas, J.B., 2006. Crystallization thermometers for zircon and rutile. Contrib. Mineral. Petrol., 151, 413–433.

Whitehouse, M.J., Dunkley, D.J., Kusiak, M.A., Wilde, S.A. 2019. On the true antiquity of Eoarchean chemofossils – assessing the claim for Earth's oldest biogenic graphite in the Saglek Block of Labrador. Precambrian Research 323, 70-81.

Zack, T., Moraes, B., Kronz, A., 2004. Temperature dependence of Zr in Rutile: empirical calibration of a rutile thermometer. Contrib. Mineral. Petrol., 148, 471–488.

FIGURE CAPTIONS

Figure 1. Simplified map of the northwestern Superior Province, with the location of the town of Inukjuak (gray dot) and the study area (yellow star) highlighted. (For interpretation of the references to color in this figure legend, the reader is referred to the web version of this article.)

Figure. 2. Regional geologic map (after Simard, 2003) showing the geological context of the ancient supracrustal remnants of the Innuksuac Complex. The study area is outlined by the rectangle (see Figure 3). Rock suites that have not been substantially characterized are shown in gray. (For interpretation of the references to color in this figure legend, the reader is referred to the web version of this article.)

Figure 3. Local geologic map showing the main lithologies discussed herein. Samples described in this work are represented by large black dots, additional samples with geochemical data are represented by small white dots, and samples from other studies are represented by small gray points (see Supplementary Information in Cates et al. 2013 for reported data tables). (For interpretation of the references to color in this figure legend, the reader is referred to the web version of this article.)

Figure 4. Field photographs of the main lithologies discussed in this work. The Voizel suite is represented by sample IN12041 (hammer for scale, ~30 cm); Ukaliq enclaves are exemplified by sample IN12042 (as a white gneiss that cross-cuts amphibolite; 1 m hammer for scale); an example of the Central Tonalitic Gneiss is from sample IN12012 (hammer for scale); and the Boizard suite is represented by IN12054 (pen for scale, 10 cm). (For interpretation of the colors in this figure, the reader is referred to the web version of this article.)

Figure 5. Back-scatter electron and cathodoluminescence paired images of representative zircon grains reported in this work (a-f). (a) Example of a euhedral, igneous zircon; note rim with bright CL response. (b) Example of an igneous core with an overgrown metamorphic rim. (c) Example

of a rounded, inherited core surrounded by an igneous overgrowth. (d) Example of a zircon with a texture typical of metamictization. (e) Zircon with a geochronology spot that has overlapped a fracture. (f) Zircon with a texture that suggests intense metamictization and/or hydrothermal alteration. Please see **Supplementary Figures S1** for the complete documentation of these samples.

Figure 6. Back-scatter electron images illustrating the textural relationships in four representative samples discussed in the text. (**a**) Meta-conglomerate sample ***IN14032A*** shows the mineral assemblage anthophyllite (Anth) + muscovite (Ms) + stilpnomelane (Stp) + quartz (Qz) + rutile (Rt). Anthophyllite is replaced by the assemblage chlorite + talc (Chl + Tc). (**b**) Boizard suite granite sample IN12016 contains the mineral assemblage chlorite (Chl) + epidote (Epi) + titanite (Ttn) + albite (Ab) + quartz (Qz). (**c**) The grey gneiss sample IN14036 shows the mineral assemblage biotite (Bt) + muscovite (Ms) + plagioclase (Pl) + quartz (Qz). Biotite is replaced by chlorite + titanite (Chl + Ttn). (**d**) The Voizel tonalite sample IN12044 contains the mineral assemblage biotite (Bt) + K-feldspar (Kfs) + plagioclase (Pl) + quartz (Qz) + apatite (Ap). Biotite is replaced by chlorite + titanite (Chl + Ttn) and albite contains small zoisite (Zo) grains.

Figure 7. Classification of samples based on normative anorthite, albite, and orthoclase compositions. Fields from Barker (1979). CTG samples are red, Voizel samples are green, Boizard samples are blue, and supracrustals and USB enclaves are purple. Numbers refer to the last two-digits of the sample identifiers in **Supplementary Table S1**. (For interpretation of the references to color in this figure legend, the reader is referred to the web version of this article.)

Figure 8. (top) Chondrite-normalized (Anders and Grevesse, 1989) REE plot; (bottom) Primitive Mantle-normalized (McDonough, 1992) multi-element plot. Color coding of the samples as in

1122 Figure 7 (**Supplementary Table S1**). (For interpretation of the references to color in this figure
1123 legend, the reader is referred to the web version of this article.)
1124
1125 **Figure 9. (a)** Light-colored quartz-rich rocks below the belt of ultramafic boudins in the northern
1126 Ukaliq supracrustal belt. Significantly, the quartz-rich rocks appear to show a progression from
1127 detrital quartzites to meta-cherts with magnetite-bearing laminae higher up. Sample location of
1128 IN14032A is annotated in the figure. **(b)** Close-up view of the quartz-rich rocks of probable
1129 detrital origin (i.e. quartzite proper). Note subtle aspects of the relict layering suggesting both
1130 grading and truncations. The greenish color is probably due to calc-silicates. **(c)** Mesoscopic
1131 view of highly deformed amphibolites and supracrustal gneiss, with strong boudinage of the
1132 more competent layers. Gneissosity has been pulled into the boudin necks and folded, whereas
1133 quartz-feldspar veins and pods fill discontinuities and areas of strong local extension. **(d)** Quartz-
1134 biotite schist at the base of the ultramafic body (***IN14032A***; labelled) for which detrital zircon U-
1135 Pb geochronology was attempted. These various outcrop-scale structures illustrate the structural
1136 style of the Ukaliq supracrustal belt, with the boudins being analogous to the larger ultramafic
1137 bodies in the wider area, and the quartz veins representing late Neoarchean granitic pegmatites
1138 that intruded late during the boudinage forming deformation. (For interpretation of the references
1139 to color in this figure, the reader is referred to the web version of this article.)

1140 **Figure 10.** U-Pb zircon geochronology expressed in Tera-Wasserburg plots for Central Tonalitic
1141 Gneiss samples (IN05001, IN12012, IN14035); gray ellipses not included in the weighted
1142 average $^{207}Pb/^{206}Pb$ age.
1143

Figure 11. U-Pb zircon geochronology for Voizel suite samples investigated in this work; gray ellipses not included in weighted mean or upper intercept age calculations.

Figure 12. Boizard suite U-Pb zircon geochronology; gray ellipses not included in weighted mean $^{207}Pb/^{206}Pb$ age.

Figure 13. U-Pb zircon geochronology for various supracrustal (NSB and USB) and USB intrusion samples; gray ellipses not included in weighted mean or upper intercept age calculations.

Figure 14. (a.) REE data plotted for zircons used in the lattice-strain partitioning modeling work described herein. (b) Onuma diagrams of selected zircons from TTG and Voizel samples showing R^2 fitting values (see Mojzsis et al. 2014 and references therein). Colors correspond to the calculated partition values for a particular grain using its host rock, and the model best-fit line. (For interpretation of the references to color in this figure legend, the reader is referred to the web version of this article.)

SUPPLEMENTARY ONLINE INFORMATION

SUPPLEMENTARY FIGURES

Figures S1. Back-scatter electron and cathodoluminescence paired images of zircon grains used in geochronological and trace-element analysis, labeled with ion microprobe spot and $^{207}Pb/^{206}Pb$ age. Please see **Supplementary Data Table S2** for specific assignments of age spots to zircons.

Figure S2. Field photos of the CTG: above, sample IN05001 (person and backpack for scale); below, sample IN12012 (hammer 30 cm for scale).

Figure S3. Field photos of the CTG: above, sample IN05001 (person and backpack for scale); below, sample IN12012 (hammer 30 cm for scale).

Figure S4a. Field photos of the Voizel suite: both pictures sample IN12014 (above: hammer and person for scale; below: field of view at bottom of photo approximately 4m).

Figure S4b. Field photos of the Voizel suite: above, sample IN12027 (hammer for scale); below, sample IN12041 (hammer for scale).

Figure S4c. Field photos of the Voizel suite: sample IN12046 (field of view at bottom of photo approximately 1.5m).

Figure S4d. Field photos of the Voizel suite: both pictures sample IN12050 (hammers 30 cm for scale).

Figure S5a. Field photos of the Boizard suite: sample IN12016 (knife 8 cm for scale).

Figure S5b. Field photos of the Boizard suite: both pictures sample IN12054 (pens for scale).

Figure S6. Field photos of USB enclaves: above, sample IN12042 (as white gneiss cross-cutting amphibolite and $A_{voi;}$ sledgehammer for scale); below, sample IN12053 (clipboard and sledgehammer ~1m for scale).

Figure S7. Field location of TTG mylonitic gneiss sample IN14036

SUPPLEMENTARY TABLES

Table S1. Data used for geochemical analysis; oxides reported in weight percentages and trace elements in ppm; CTG = red, Voizel = green, Boizard = blue, USB enclaves = purple.

Table S2. Data used for geochronological analysis; CTG = red, Voizel = green, Boizard = blue, USB enclaves = purple.

Table S3. Data used for zircon trace-element analysis; CTG = red, Voizel = green.

Table S4. Results of Zr-in-rutile analyses.

Figure 1

Click here to download high resolution image

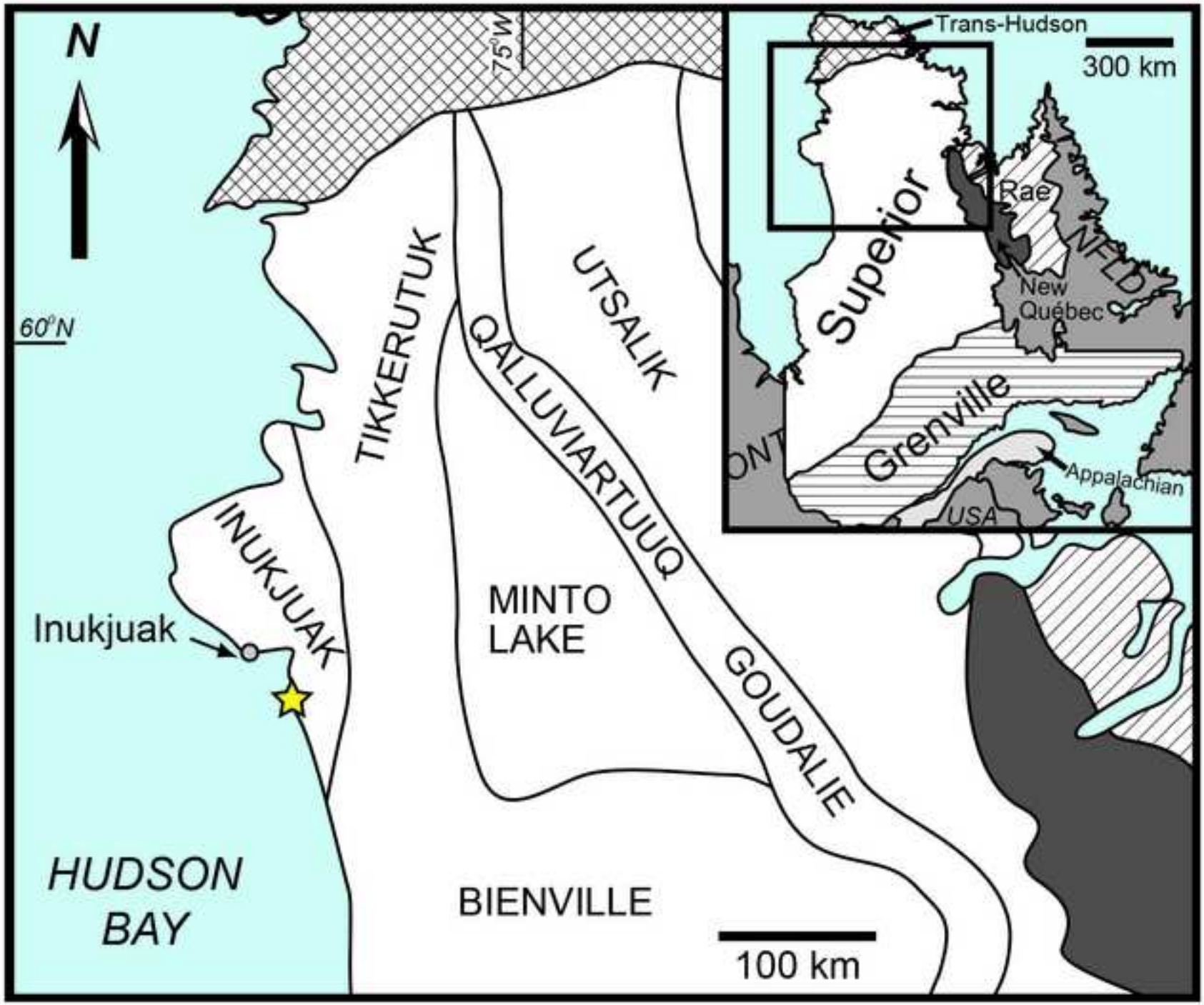

Figure 2

Click here to download high resolution image

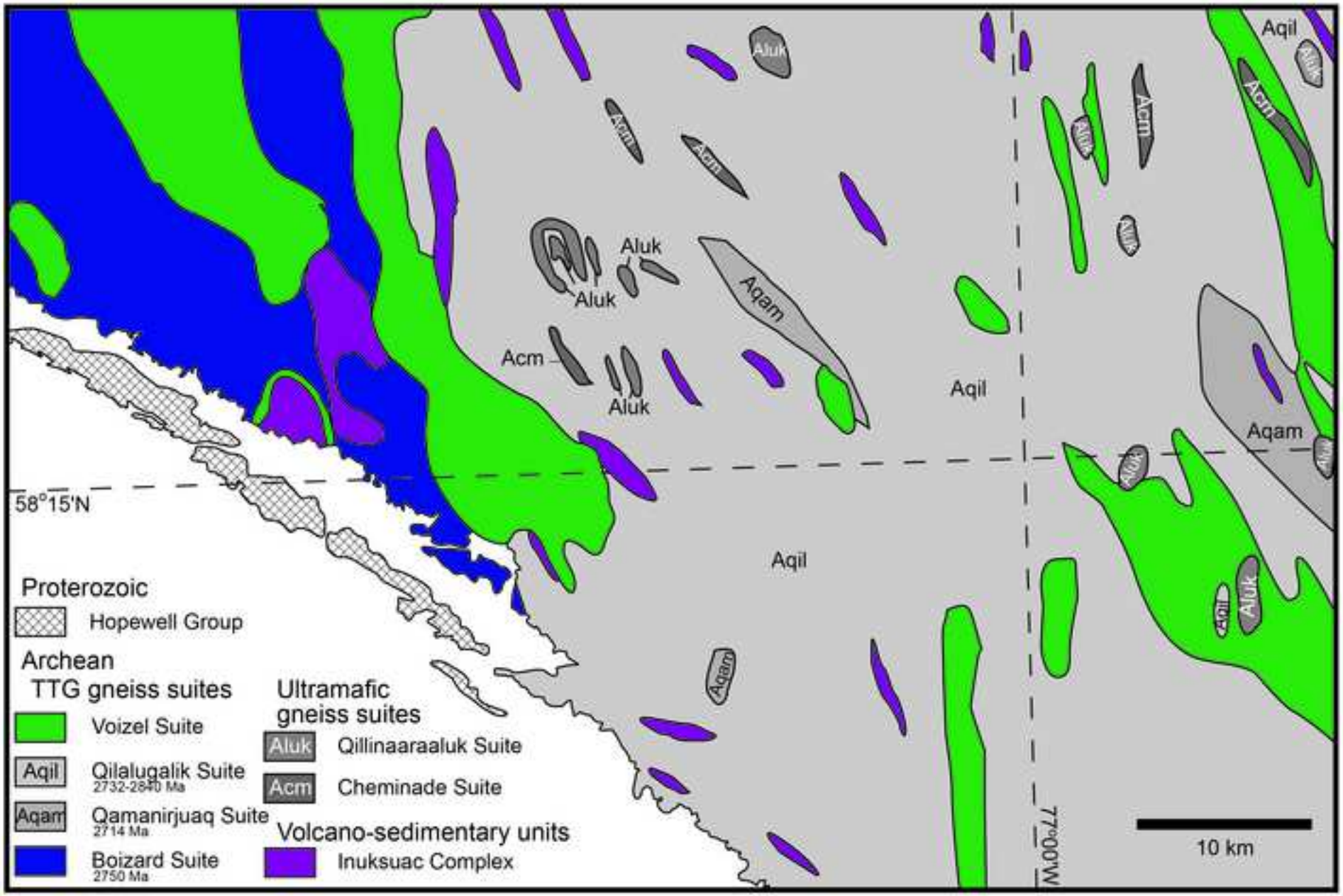

Figure 3

Click here to download high resolution image

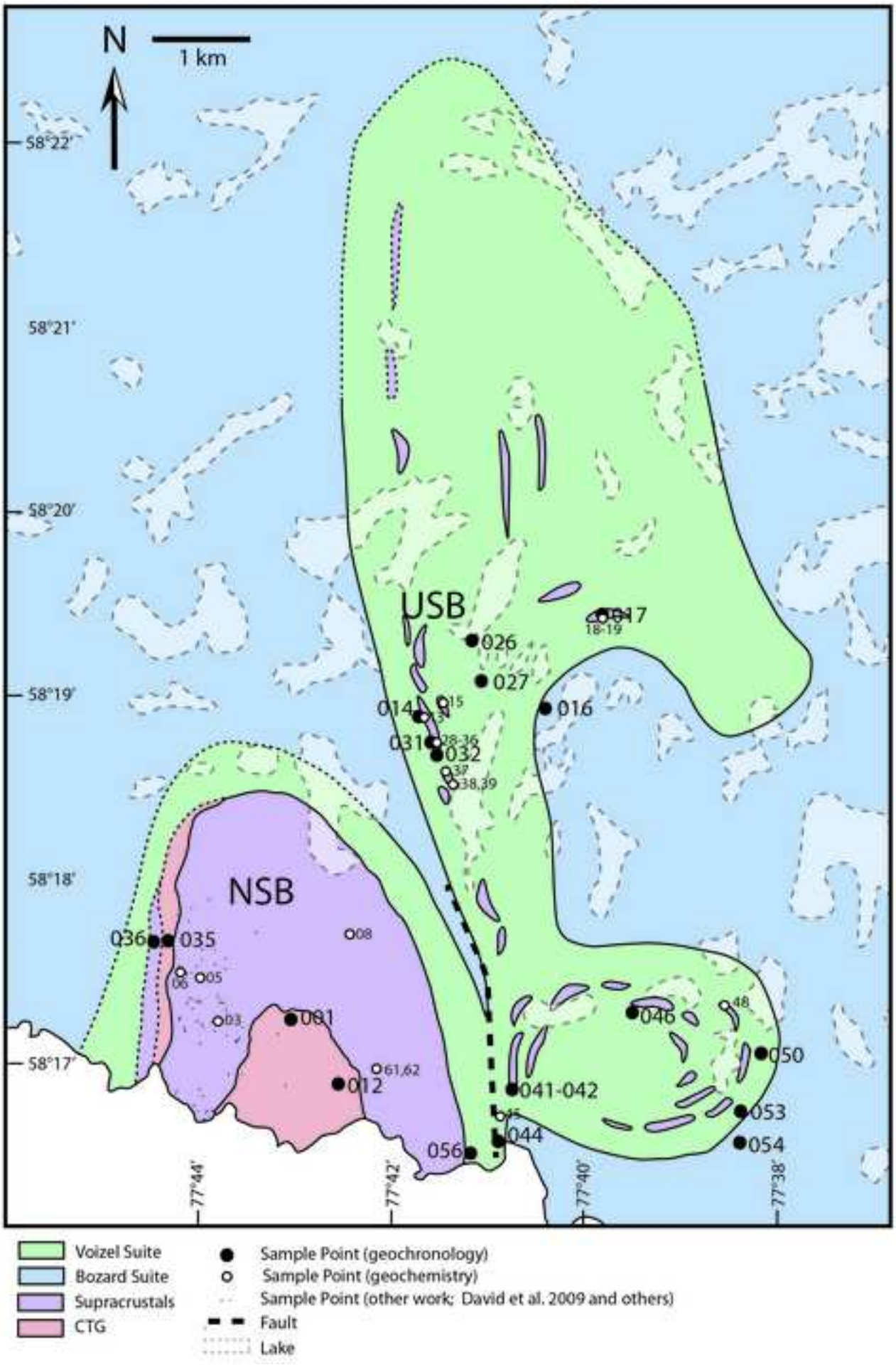

Figure 4

Click here to download high resolution image

Figure 5

Click here to download high resolution image

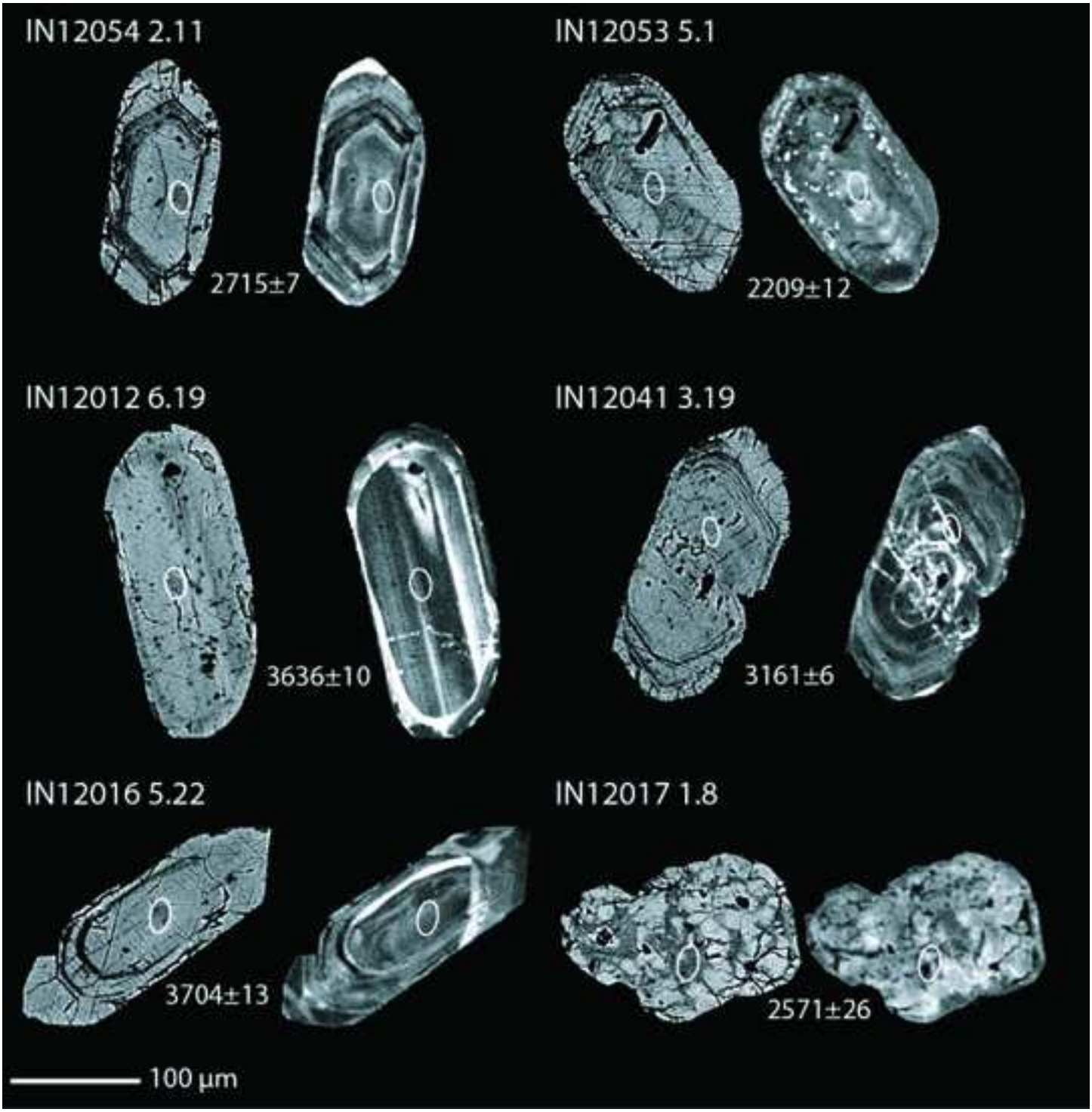

REVISED Figure 6

Click here to download high resolution image

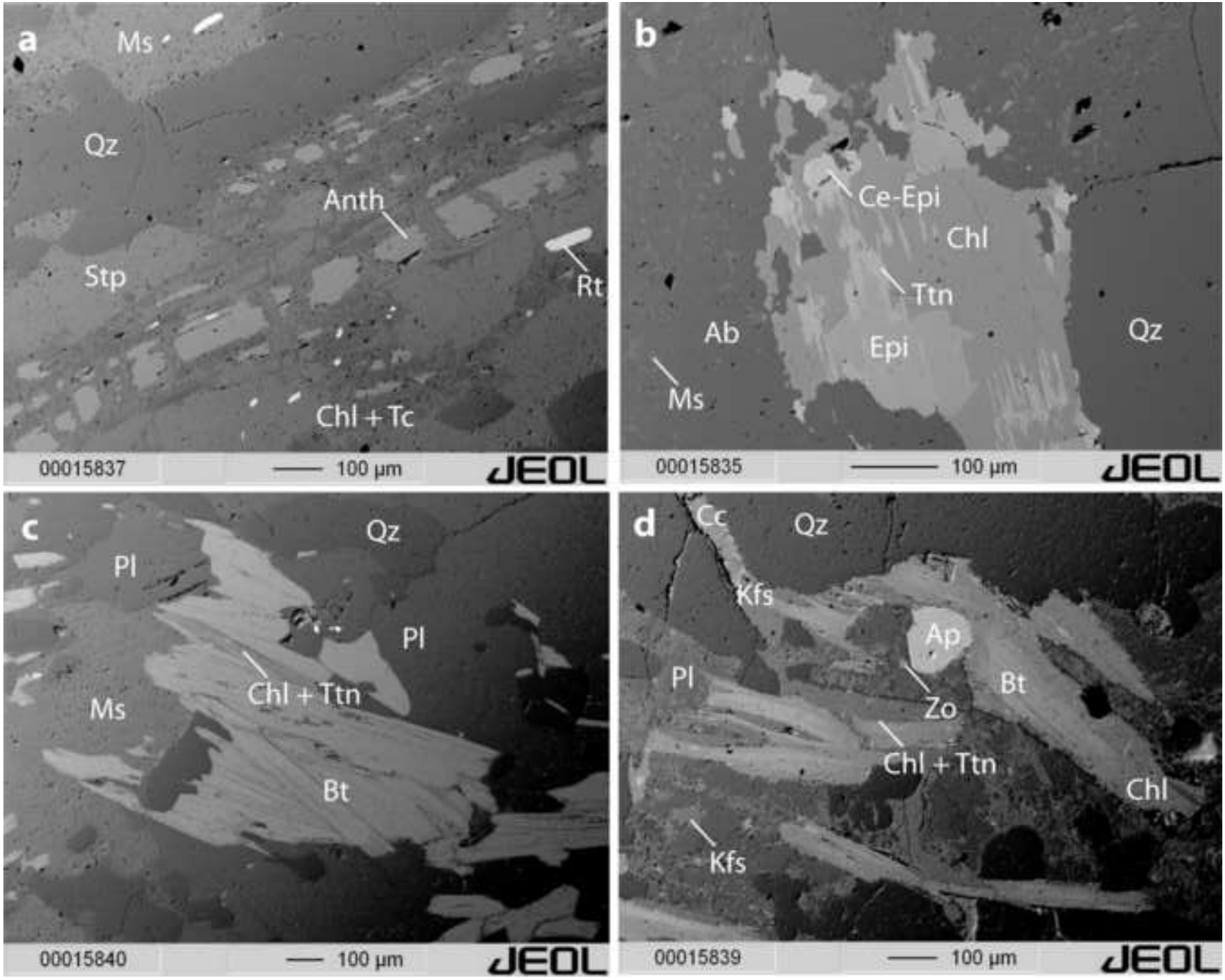

REVISED Figure 7

Click here to download high resolution image

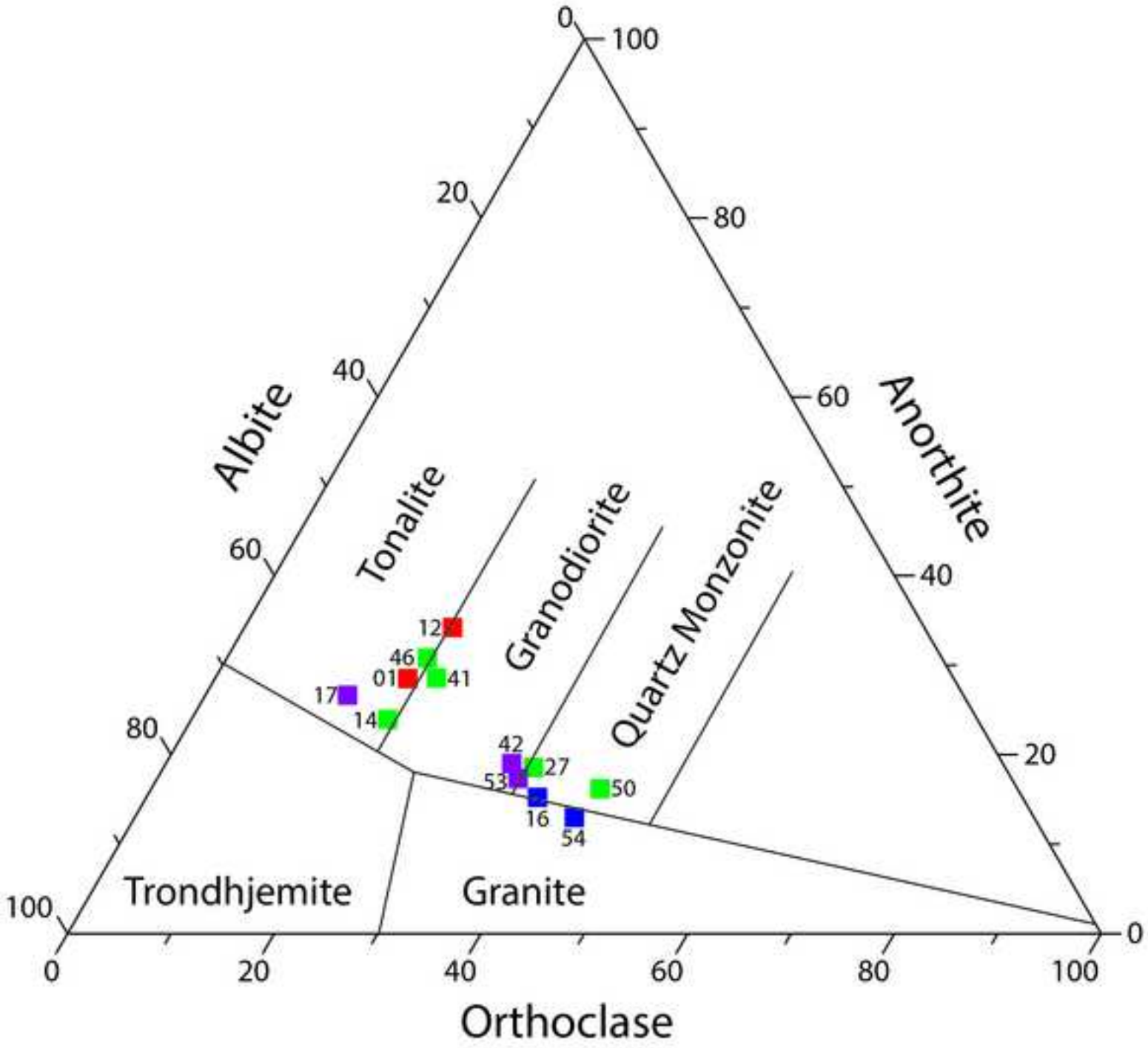

REVISED Figure 8

Click here to download high resolution image

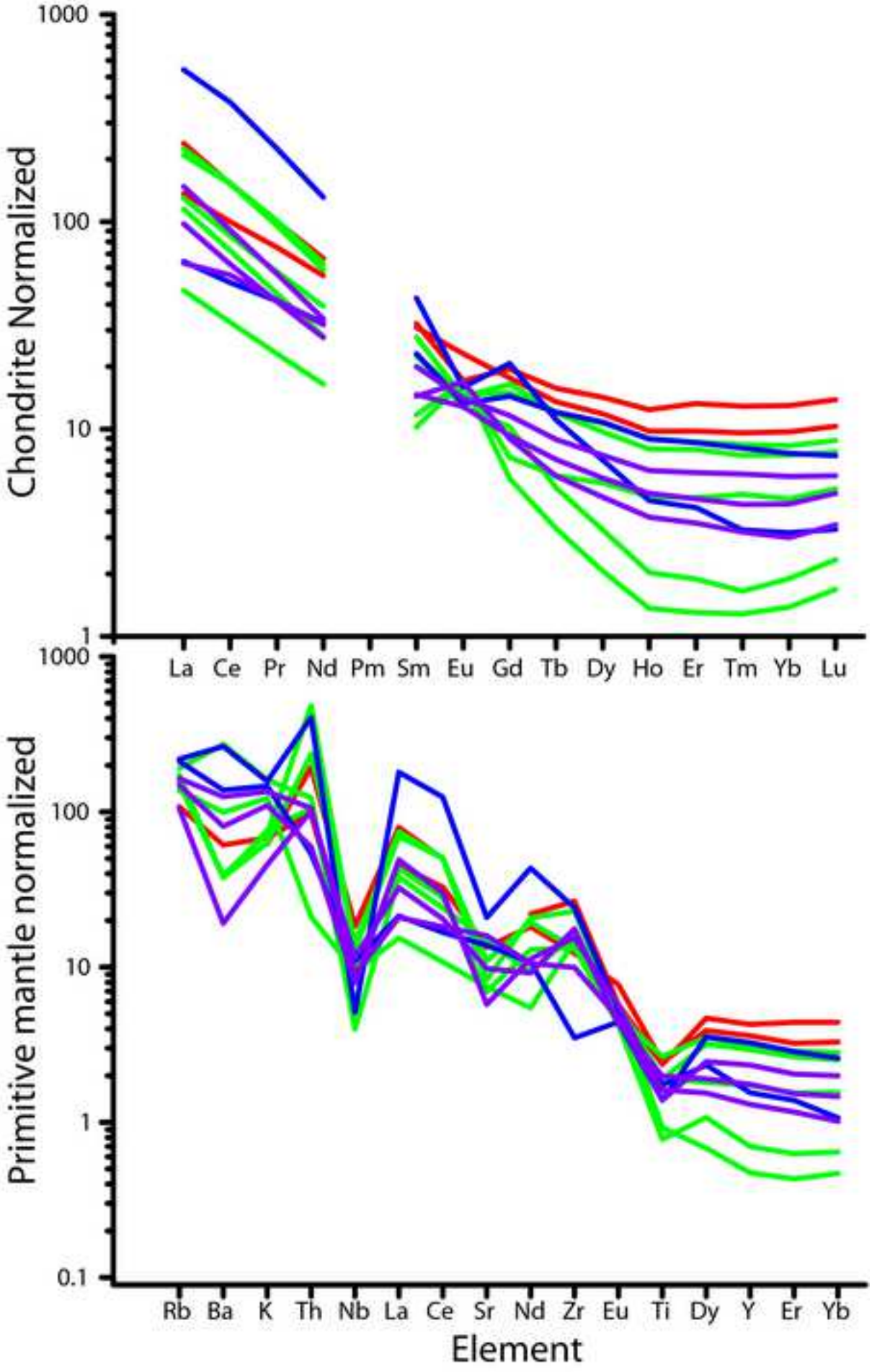

REVISED Figure 9

Click here to download high resolution image

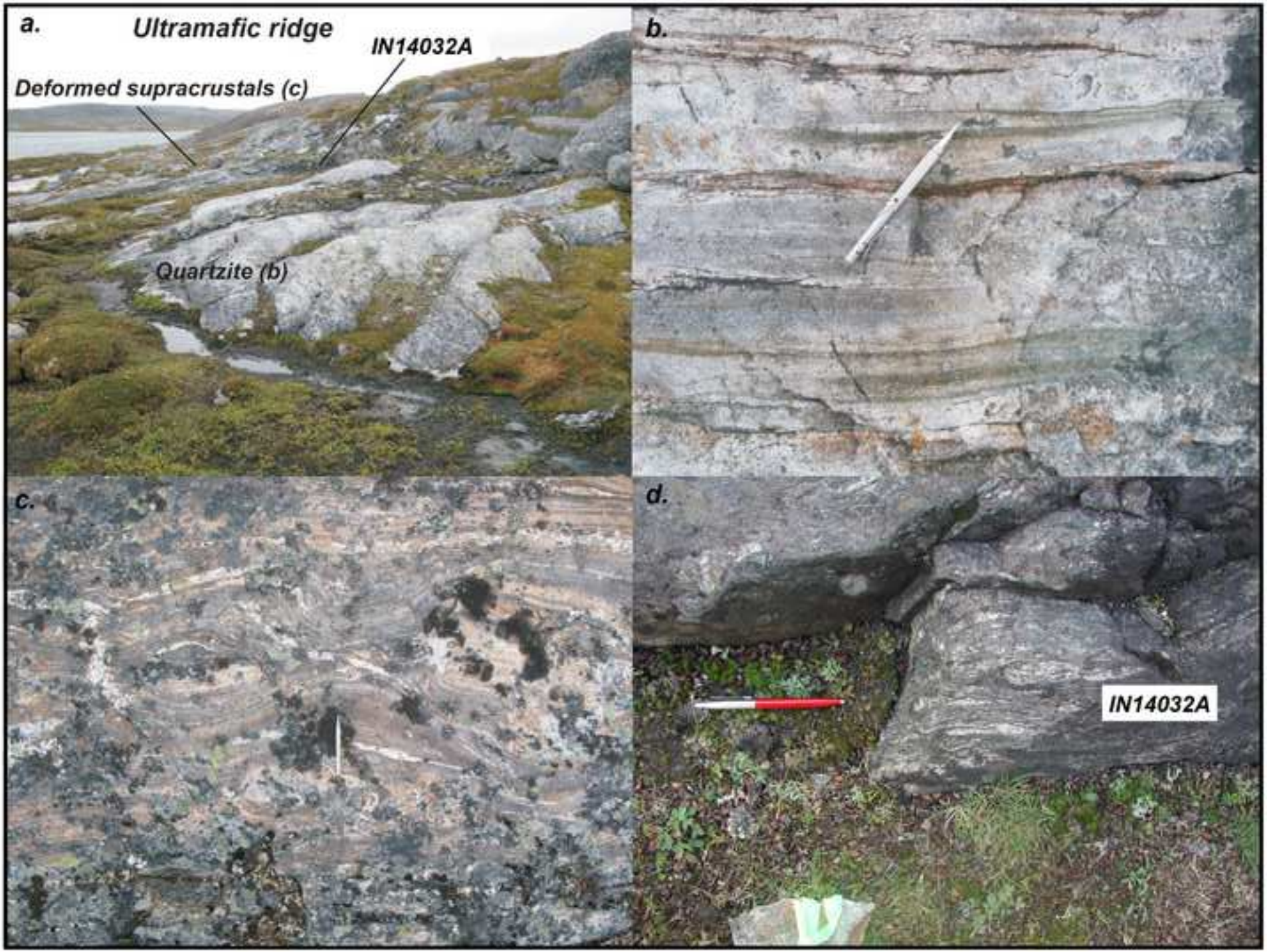

Figure 10

Click here to download high resolution image

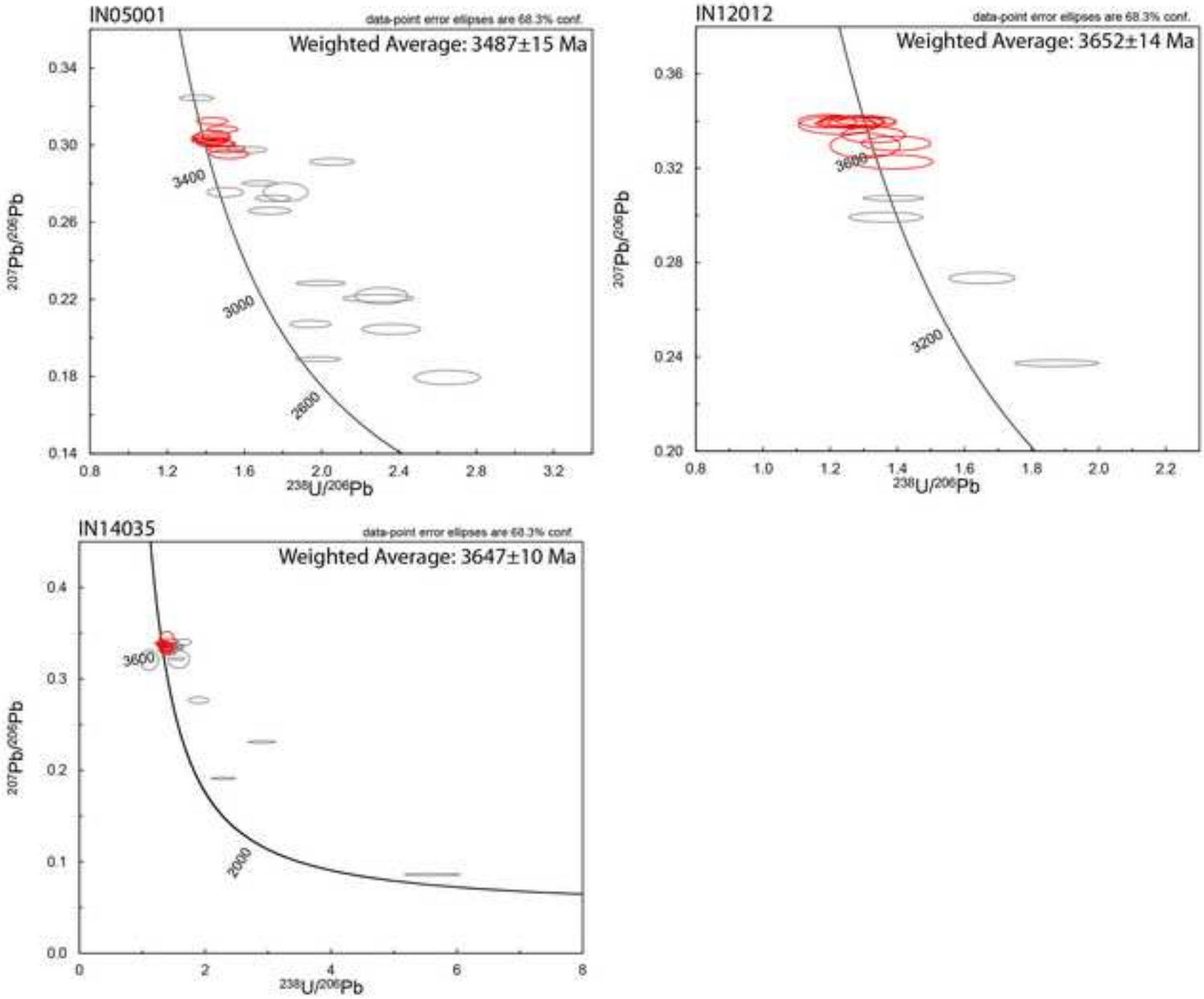

Figure 11

Click here to download high resolution image

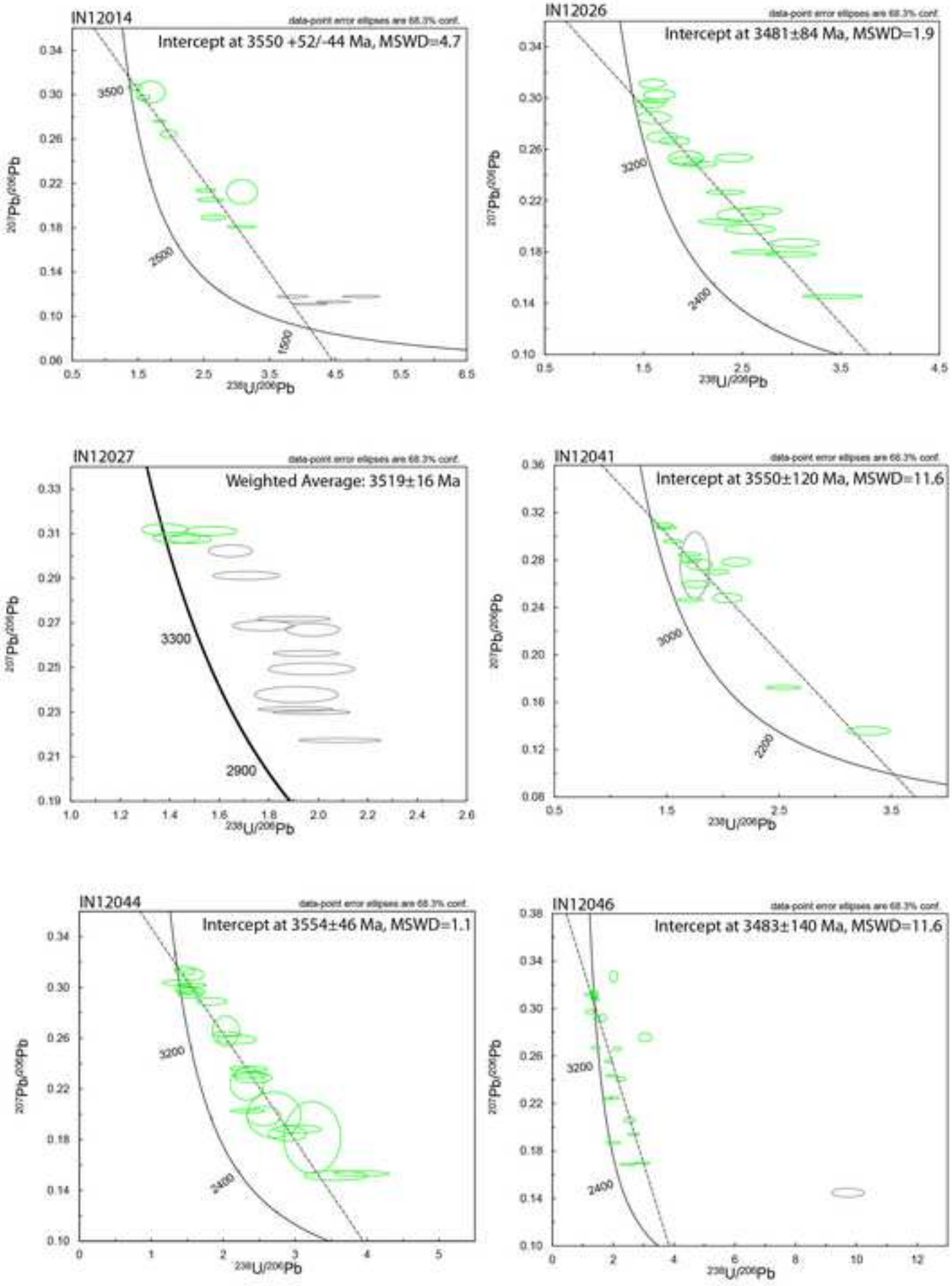

Figure 11 continued

Click here to download high resolution image

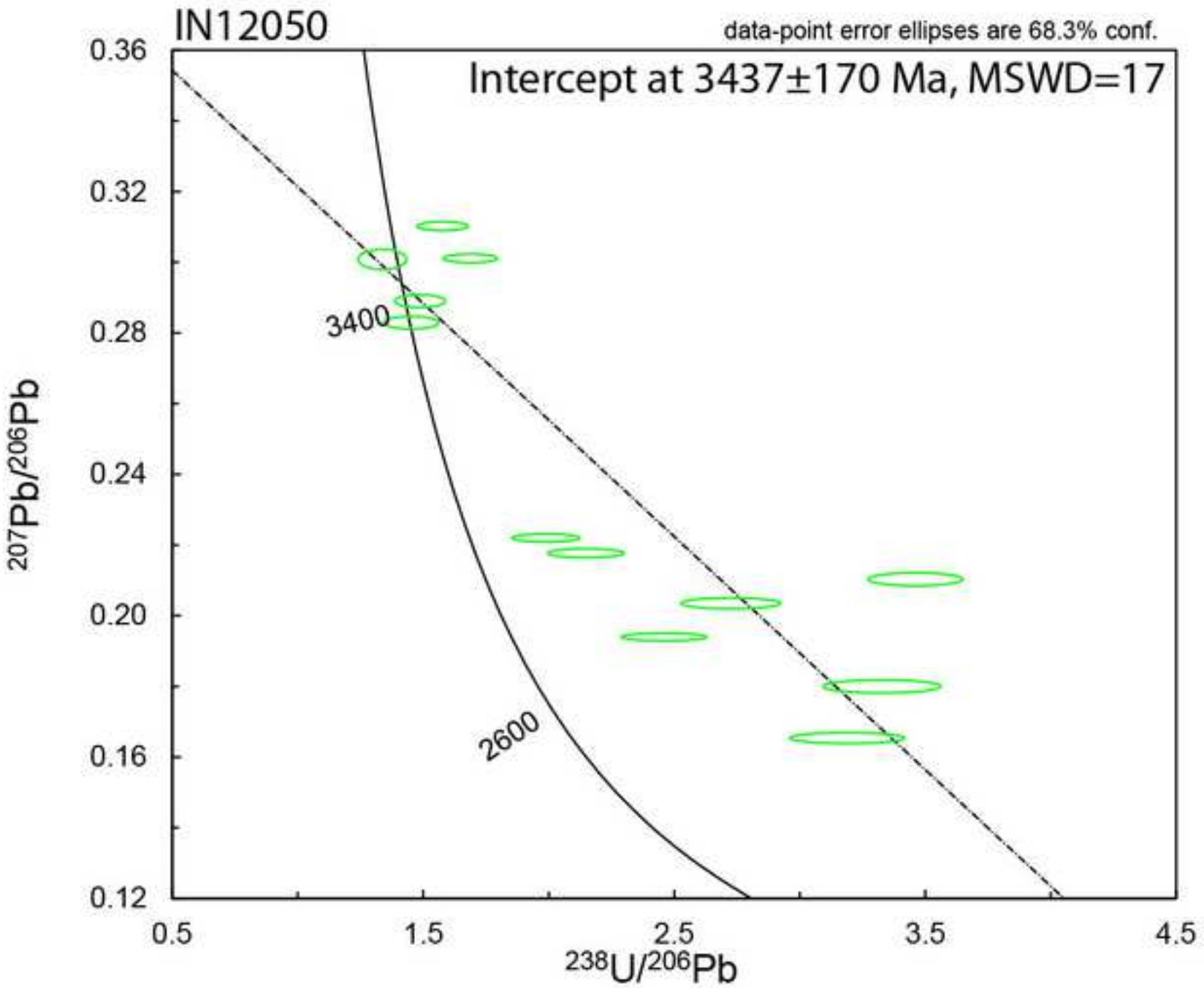

Figure 12

Click here to download high resolution image

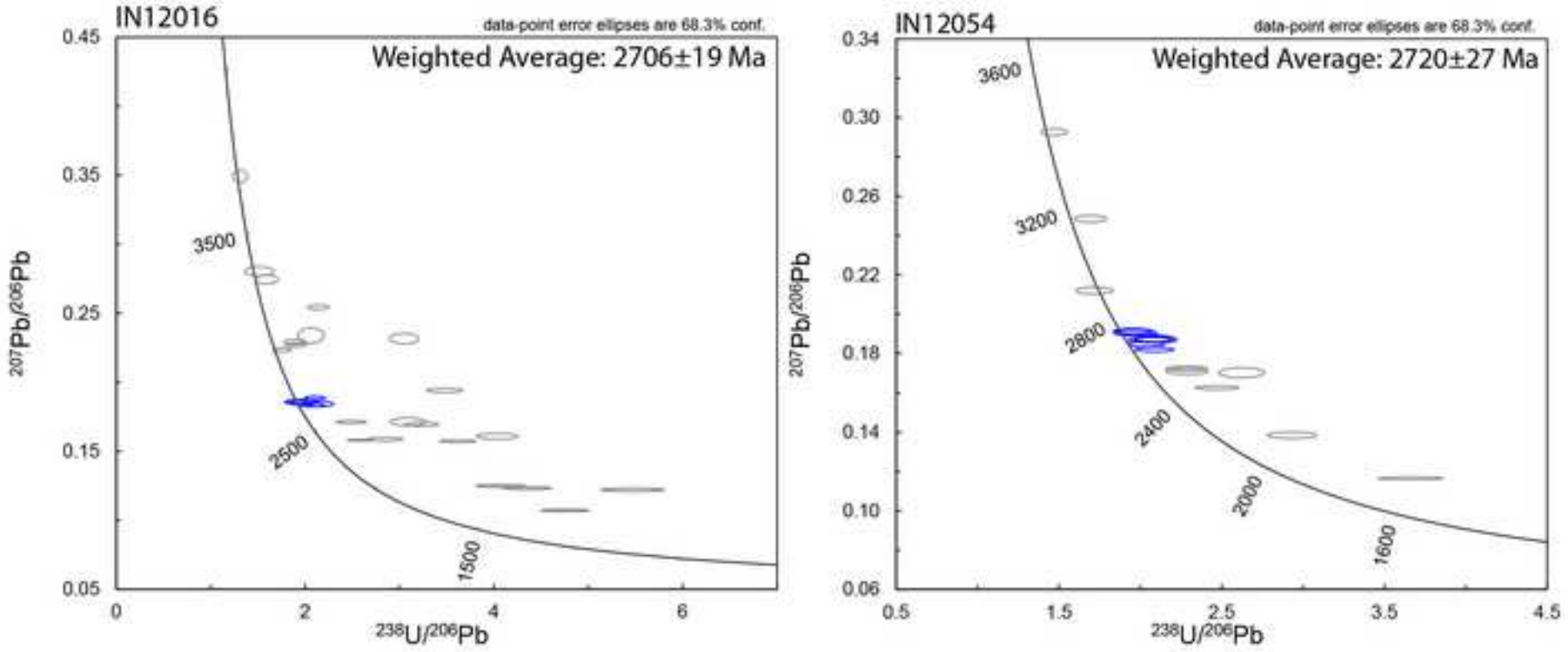

REVISED Figure 13

Click here to download high resolution image

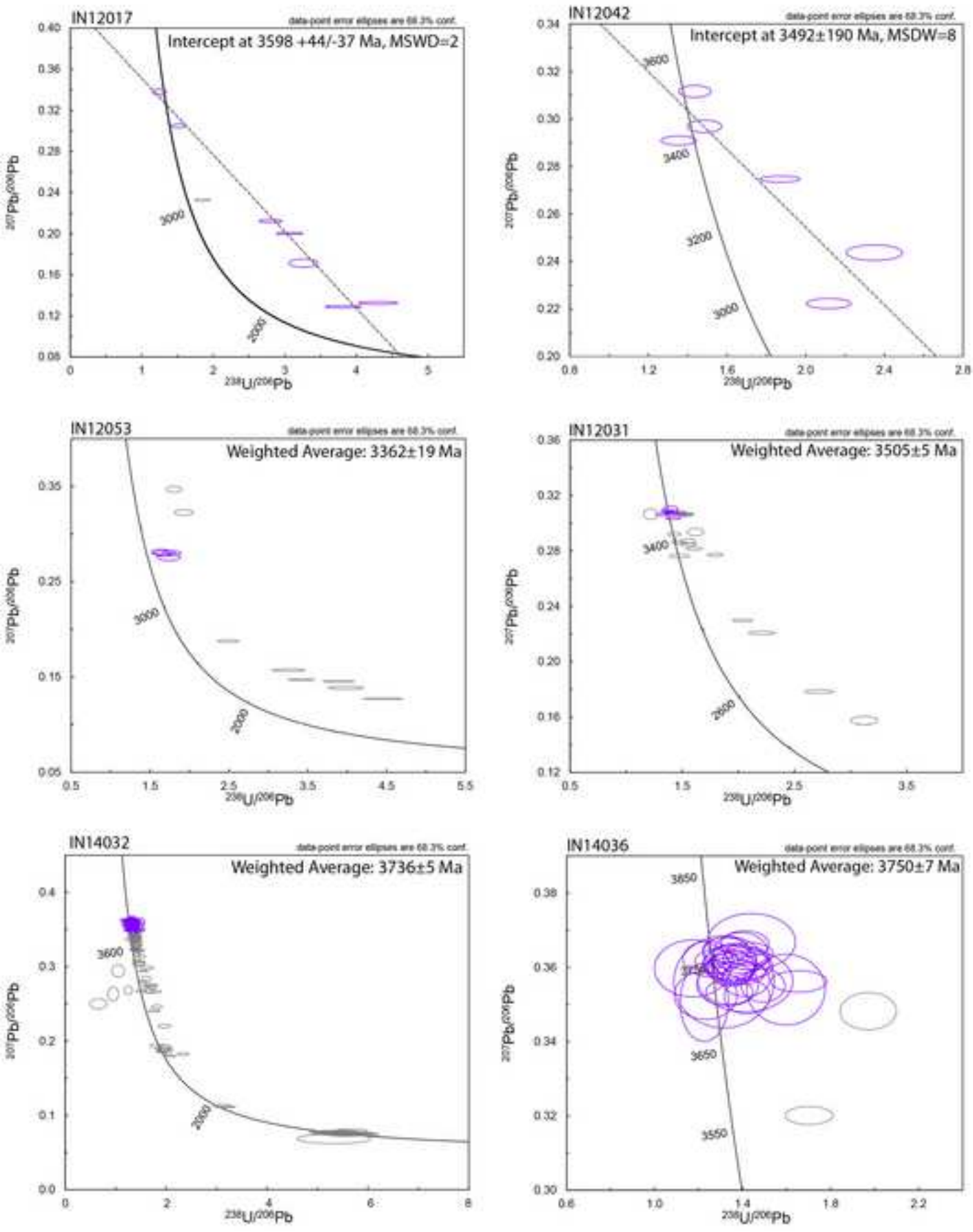

Figure 14

Click here to download high resolution image